2009

A cavity-backed coplanar waveguide slot antenna array

James W. Mcknight
University of South Florida

A Cavity-backed Coplanar Waveguide Slot Antenna Array

by

James W. McKnight

A thesis submitted in partial fulfillment
of the requirements of the degree of
Master of Science in Electrical Engineering
College of Engineering
University of South Florida

Major Professor: Thomas M. Weller, Ph.D.
Jing Wang, Ph.D.
Kenneth Buckle, Ph.D.

Date of Approval:
October 14, 2009

Keywords: CPW slot, cpw-fed slot, reflector, bi-directional feed, series feed, beam-steering, C-band

TABLE OF CONTENTS

LIST OF TABLES

LIST OF FIGURES

A Cavity-backed Coplanar Waveguide Slot Antenna Array

James McKnight

ABSTRACT

In this thesis, a cavity-backed slot antenna array is designed for relatively wide instantaneous bandwidth, high gain and low sidelobes. The array consists of four, rectangular, slot elements, arranged side-by-side in a linear array and developed around 5GHz. Two feed points, at opposing sides of the printed array, each excite two of the slot elements through a series feed. This bidirectional feed presents symmetry to the design and prevents the tendency of beam-drift versus frequency as is common with many series-fed arrays. While being fed in-phase, the array will maintain boresight at broadside over the entire operating bandwidth. Also, the additional port allows for the potential introduction of a phase offset and, therefore, beam tilt. Finally, the printed array is designed to function within a quarter-wave, metallic cavity to achieve unidirectional radiation and improve gain.

CHAPTER 1

INTRODUCTION

1.1 Overview

Among the current driving forces in wireless communications, there is a need for compact, efficient, inexpensive and reproducible antennas. In some instances, particularly long-distance applications, radiators with directive, high-gain characteristics are necessary. This work proposes a cavity-backed slot array to that end. The array consists of four wavelength-long, rectangular slots which, in concert, will yield a high gain pattern and low sidelobes. Additionally, the array is excited with anti-symmetric feeds which will prevent beam drift over frequency. The bidirectional radiation array is placed within a metallic cavity to attain uni-directional radiation and further improve gain.

1.2 Motivation

Slot antennas are known for their sturdy, planar structure and have long been a prominent part of wireless systems. Their structure is complementary to the printed dipole and a single radiating slot will generate a linearly polarized, but broad, far-field pattern. Coplanar waveguide (CPW) feeds are a natural choice for printed slots as they allow the entirety of the design to be fabricated on a single layer, in a single process.

Often, an array of elements is employed to improve directionality and concentrate energy into a narrow pattern. The array is based on two array segments each composed of two slots and each with their own feed. When all elements are fed in-phase, the array will produce a beam at broadside. However, because the design is based on dimensions that are proportional to the operational, center frequency (f_c), the beam may be sensitive to changes in frequency and drift away from broadside as the frequency moves away from f_c. The symmetry of the array and opposing feeds circumvents this potential drawback and allows the beam stay fixed at broadside over a range of frequencies. A phase shifter, external to this device, could offset the phase of one port, and allow the beam to be electronically tilted about broadside (Figure 1.1).

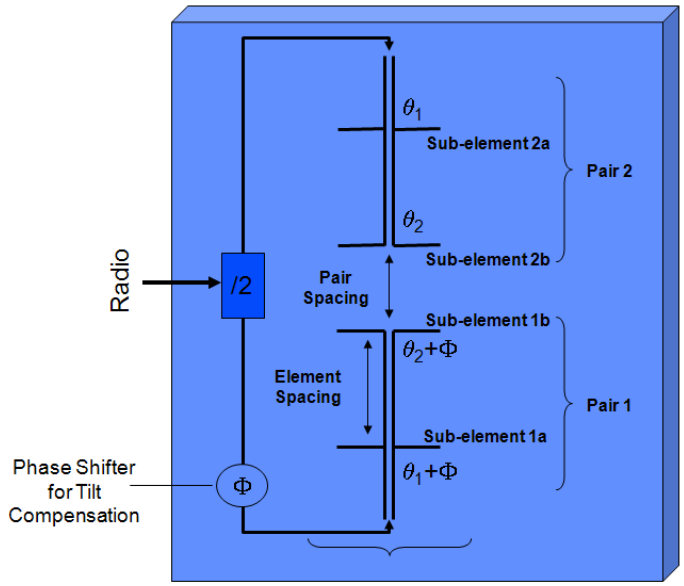

Figure 1.1 - Proposed Planar Array.

The inherent bidirectional nature of the slot's radiation may be wasted if communication is only required in one direction. If the antenna is mounted on a

structure, that backside radiation would be radiating into the structure which could cause significant field cancellation. By properly positioning a metallic reflector or cavity behind the slot, the backside radiation can be recuperated and added constructively to form a uni-directional and directive, major beam.

1.3 Thesis Organization

This work is organized into six chapters. Chapter 1 introduces the work, its motivation and contributions. Chapter 2 is the background/literature search and examines similar and/or contributing works including: rectangular slots, printed slots and slot arrays. Also in this chapter, a theoretical analysis is presented for aperture antennas. Feeding the slot is of issue, so slot feeds are briefly covered here too.

Chapter 3 details the design of a wavelength-long rectangular slot element that the slot array is based around. Its various dimensions can be tuned to have strong resonance over a relatively wide bandwidth. Measured and simulated results for return loss and radiation pattern are given.

Chapter 4 introduces the series-fed array of four elements. The array is built around the single slot developed in Chapter 3 in order to increase the antenna gain. The chapter begins with an investigation of basic array theory to understand how the linear array will dictate the radiation pattern. Other design considerations are addressed here including: mutual impedance, the CPW feed effects and impedance matching.

Finally, Chapter 5 incorporates the metallic cavity. The array structure of Chapter 4 must be tuned to function properly within the cavity. The design becomes more complicated with the addition of the cavity, so simulations are done in Ansoft's HFSS.

1.4 Contributions

This work is intended as a proof of concept that a slot array can be designed to have high gain and a unidirectional radiation over a range of frequencies. To prevent the tendency of series-fed arrays to beam-drift over frequency, an anti-symmetric will keep radiation fixed at broadside over the entire operating bandwidth. To the author's knowledge, it is the only series-fed slot array that maintains broadside radiation versus frequency. The additional feed point will also allow the introduction of a phase offset and, thus, beam-steering that is independent of frequency. Furthermore, the array is made to function within a metallic cavity for uni-directional radiation, increased gain and negligible sidelobes and/or backside radiation. The design is built for operation in the C-band (around 5GHz) but can be scaled to other frequencies.

CHAPTER 2

APERTURE AND SLOT ANTENNAS

2.1 Introduction

Planar antennas and, particularly, planar arrays have garnered increasing popularity in space and radar communication systems, remote sensing and radio astronomy. Their planar structure is inherently durable and low-profile, making them an ideal candidate for aircrafts where they can be flush-mounted onto the hulls [1]. In this thesis, attention is focused on slot antennas and, specifically, CPW, series-fed slot arrays.

Modern day slot antennas have their roots in rectangular waveguides but have mostly shifted to the planar form. This chapter will briefly address the assortment and evolution of slot radiators. Slots are a somewhat different breed of antennas, and, as such, a terse, theoretical analysis of the slot behavior will be presented. Some attention will also be given to the available feeding techniques for the slot.

2.2 Planar Radiators

While there are abounding variations in the family of planar radiators, most fall into one of two broader categories: patch antennas and slot antennas. Both slot and microstrip (patch) antennas are commonly formed in standard PCB substrates, making them relatively simple and cheap to produce. Each topology has its own advantages and

disadvantages, allowing the designer some flexibility. Table 2.1, below, gives a side-by-side comparison of some of the more notable features of slot and microstrip radiators.

Table 2.1 - Comparison of Microstrip Patch and Slot Antenna

Characteristic	Microstrip	Slot
Analysis and design	Easy	Easy
Fabrication	Very Easy	Very Easy
Tolerance in Fabrication	Critical	Not very critical
Profile	Thin	Thin
Shape Flexibility	Any Shape	Limited
Radiation Fields	Unidirectional	Unidirectional or Bidirectional
Polarization	Linear and Circular	Linear and Circular
Bandwidth	Narrow	Wide
Dual frequency operation	Possible	Possible
Spurious radiation	Moderate	Low
Isolation between radiating elements	Fair	Good
Frequency scanning	Easily possible	Possible
Cross-polarization level	Low	Very low
End-fire antenna	Not possible	Possible

The slot has some obvious advantages over the patch; it is relatively insensitive to the fabrication process, it can be used for bidirectional or unidirectional radiation and it is capable of wider bandwidths than the patch. It is the slot variety that will be explored in this work.

2.3 Existing Slots Antennas

Even though the basic concepts behind radiating apertures were known in the late 17th century with the work done by Huygens, they were not extensively studied and developed until World War II [2]. With work like that done by Watson [3] and Stevenson [4], slots were first used in the walls of rectangular waveguides to couple and radiate energy. Later, Orefice and Elliot [5] proved they could control antenna

parameters like external mutual coupling, input impedance and radiation pattern by adjusting the length, spacing and orientation of the slot elements within a rectangular waveguide array (Figure 2.1).

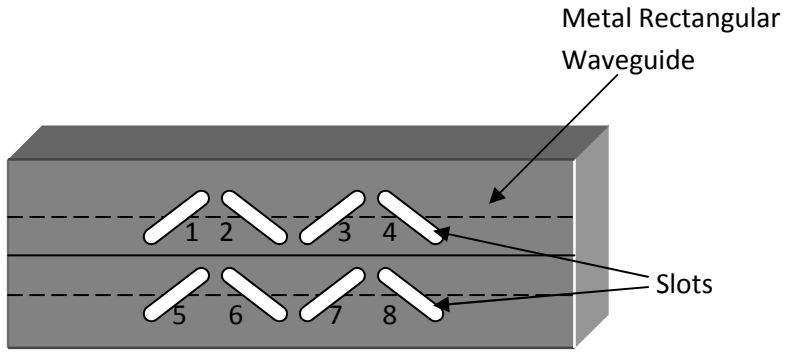

Figure 2.1 - Slot Array in a Rectangular Waveguide as Proposed by Orefice and Elliot.

Rectangular and circular waveguides still maintain some special-use applications today, but slots have mostly made the transformation to the planar form as the high-tech trends have called for low-profile, compact structures. Rectangular slots, like those originally used in rectangular waveguides [5-8], are the most fundamental of slot shapes with only two adjustable dimensions. They are still employed in modern, planar designs. Yoshimura's work [9] showed the rectangular slot could feasibly be fed with a microstrip and that a flat reflector behind the slot could salvage backside radiation. In the same work, it was shown directionality could be further enhanced with an array of said elements. Nesic presented a printed, linear slot array excited by a CPW [10]. He noted that the CPW feed can be easily branched for a two-dimension planar array.

Bow-tie slots, like that introduced by Soliman et al [16], are discernibly more complex than the rectangular slots, but with advantages. Soliman showed that the bow-

tie structures, shown in Figure 2.2, can achieve very large bandwidths, have an input impedance which can be easily controlled and a dipole-like, linearly polarized radiation pattern. Similar CPW-fed bow-tie antennas [12-18] use various techniques to obtain ultra-wide bandwidths and/or miniaturization. Other slot configurations like the annular slot, spiral slot and are compact but are not fit for this work.

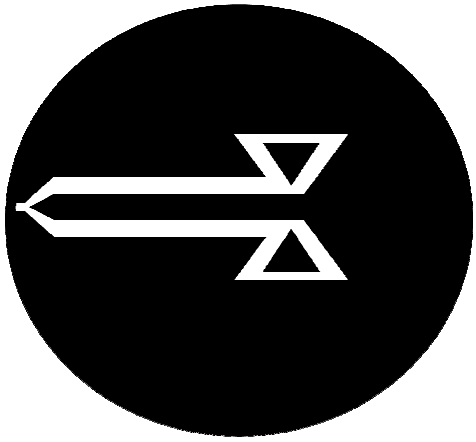

Figure 2.2 - Soliman's Bow-tie Slot.

Using these various slot configurations and feeding techniques, linear and planar slot arrays can be formed by feeding multiple structures systematically; attention will be given to arrays formed from rectangular slots.

The hybrid slot array (HSA) and log-periodic array (LPSA) designs (Figure 2.4) by A. Bhobe are constructed around the rectangular slot element and center-fed with CPW as Nesic first proposed[19]. The HSA and LPSA designs achieved bandwidths of nearly 60% demonstrating that the rectangular slot can be designed for

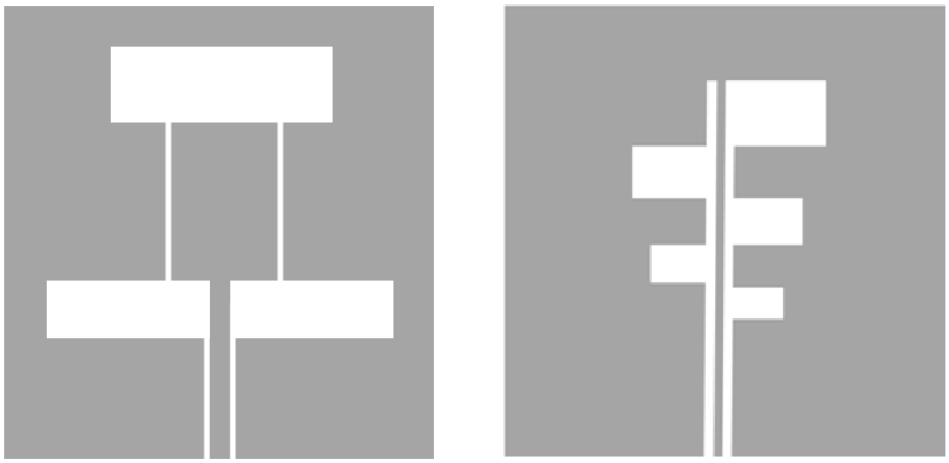

Figure 2.3 - Hybrid Slot Array (a) and Log Periodic Slot Array (b).

Kobayashi used CPW to feed 1-D and 2-D arrays of slots and showed that the gain of the major lobe could be significantly increased with additional elements, up to six, in a linear array. However, increasing from six to eight elements did not improve gain and most designs had low efficiency [20]. Huang, and others [21], similarly used a single, series CPW line to uniformly excite a linear array of four elements which yielded a narrow, bidirectional E-beam at broadside. Their approach paid particular attention to the effects of mutual coupling and factored those effects into their design process. The Series-Feed Collinear Slot Array [22] used open-ended and short-ended stubs to set the field distributions of six, series-fed slots. The arrays were capable of up to 20% bandwidths around 5GHz. They also showed that a flat reflector could suppress backside radiation of the array (20dB down from the front) and significantly increase the peak gain. The Open-Ended Rampart Slot Array Antenna is also fed with CPW and easily feeds the six elements of the array. Also based in the C-band, the array achieved up to 11% bandwidth with up to 9dBi of gain.

2.4 Analysis of Radiators

Slots are a form of aperture antenna, which include but are not limited to: slots, horns, open-ended waveguides and lens/reflector antennas. In general, an aperture antenna is simply an arbitrary hole or opening in a metal sheet or screen through which or from which an electromagnetic (EM) field will radiate. Aperture antennas are categorically different from other antenna structures in that the EM waves produced by apertures are controlled by the openings in a metal sheet, rather than the shape of the metal alone (Figure 2.5). The shape and size of the aperture are frequency-dependent proportions which will dictate the center frequency of operation, input impedance and polarization of the EM field that can effectively radiate through it. As a result, the far-field pattern, half-power beamwidth and directivity are directly shaped by the opening and can be properly manipulated by prudent array design.

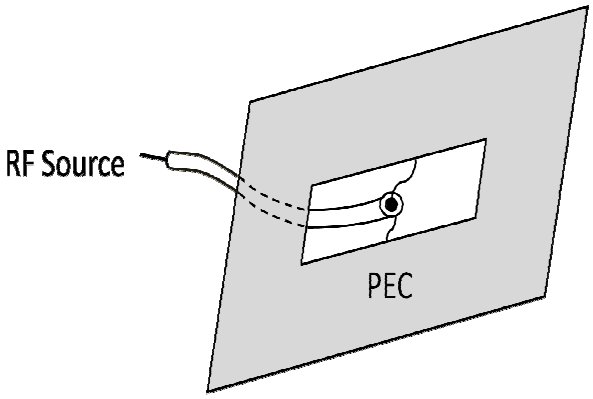

Figure 2.4 - Generic Rectangular Slot Excited by Coax.

2.4.1 Methods for Dipoles

In terms of analysis, slots must be approached somewhat differently from patches. For structures like the wire, printed dipole and patch, the radiation characteristics can be

determined once the current distribution throughout the metal can be known or approximated. The current distribution at any point on the structure is a function of space and time and can often be too complex and laborious to solve analytically. To simplify the problem, the actual current distribution can be regarded mathematically and conceptually as a collection of infinitesimal dipole sources distributed over the surface where the current of each segment can be assumed constant. The radiated field from each of these small dipoles can be calculated using closed-form or numerical techniques. By taking their linear superposition or summation, the total field radiated from the structure can then be determined for any arbitrary point *P* in the far field.

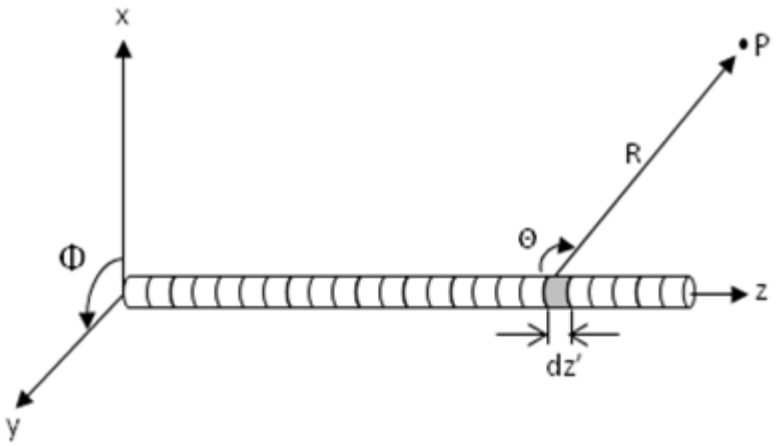

Figure 2.5 - Monopole Subdivided into Infinitesimal Segments.

An example of this technique is shown in Figure 2.6 for a simple monopole of negligible diameter. The monopole structure is subdivide into a number of infinitesimal point sources of length *dz'*. Subdivisions that tend to zero length (or volume) become more exact but, consequentially, more complicated. To be practically applied, the size of

the segments must be specific to the structure and its relative size to wavelength proportions whereby the current per segment can be considered nearly uniform.

$$dE_\theta \cong j\eta \frac{kI_e(x',y',z')e^{-jkR}}{4\pi R} sin\theta \, dz' \qquad (1)$$

$$dE_r \cong dE_r = dH_r = dH_\theta = 0 \qquad (2)$$

$$dH_\Phi \cong j\frac{kI_e(x',y',z')e^{-jkR}}{4\pi R} sin\theta \, dz' \qquad (3)$$

$$E_\theta = \int_{-l/2}^{+l/2} d\, E_\theta = j\eta \frac{ke^{-jkr}}{4\pi r} sin\theta \left[\int_{-l/2}^{+l/2} I_e(x',y',z')\, e^{jkz'\, cos\theta} dz'\right] \qquad (4)$$

Equations 1-3 give the closed form solutions of in E- and H-Fields per linear division and are valid for the far field region of the monopole of Figure 2.6. The total far-field pattern can then be obtained by summing, or integrating, the contributions from all of the infinitesimal elements, as is given in Equation 4. This approximation is valid when the diameter of the wire is negligible, much less than the operating wavelength or independent of *R* and *Φ* [1]. When the field approximation becomes multi-variable dependent, the solution difficulty is significantly compounded.

2.4.2 Apertures and the Field Equivalence Principle

An alternative method is in order for aperture antennas. In the absence of metal, no electric current flows through the slot itself. When energy is applied to the slot, the currents that flow in the metal sheet are not restricted to the edges of the slot but, instead, spread throughout the sheet. Radiation, then, takes place from both sides of the sheet. In theory, the radiated field could be resolved by directly solving the surface currents around the slot, as is done with dipole-like structures. Most slot approximations like Method of Moments (MOM) rely on the metal surrounding the slot to be of infinite extent so image

theory can be ushered in for simplification [2]. In reality, though, this is not practically realizable. A more manageable pursuit would be to reduce the area to be solved for by evaluating the fields over the aperture itself, rather than in the abundance of metal surrounding the aperture. The electric fields across the slot can be replaced with equivalent magnetic currents down its length. Magnetic currents, though artificial, help to balance Maxwell's equations and simplify the calculations required to solve for the radiated field. If the exact field were known for every point on the face of the aperture, the radiated field could also be calculated exactly. Still, the exact solutions are extremely difficult to obtain for apertures, so other approximate methods, like the field equivalence principle, are needed for simplification [23].

The field equivalence principle allows the actual sources of an EM field within a region to be replaced by equivalent, yet fictitious, sources that will produce the same fields within that region. The field equivalence principle is an expansion on Huygens' Principle which is a synthetic approximation of the fields over the aperture and considers the area of the aperture to be composed of individual point sources [1]. Each of these sources can be viewed as a primary wavefront that scatters out radially and "*can be considered to be a new source of a secondary spherical wave and that a secondary wavefront can be constructed as the envelope of these secondary spherical waves* [24]" The equivalence principle is based on the uniqueness theorem which states that "*a field in a lossy region is uniquely specified by the sources within the region plus the tangential components of the electric field over the boundary and the latter over the rest of the boundary.*"

Together, the equivalence principle and uniqueness theorem can readily facilitate an approximate solution for any field on any surface. Thus, this technique can be used to recreate the fields exterior to some closed surface if the real sources creating those fields are fully contained within that boundary and the electric and magnetic currents on that boundary satisfy the necessary boundary conditions [1]. An example is demonstrated below.

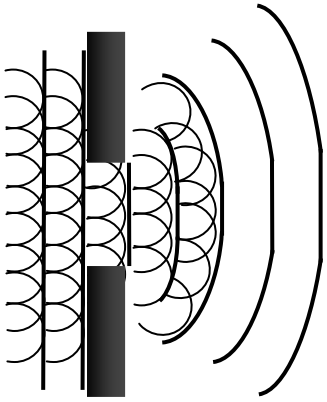

Figure 2.6 – Huygen's Field Equivalence Principle.

An arbitrary surface S in Figure 2.8(a) circumscribes a closed volume V_1 which fully encapsulates the electric and magnetic sources J_1 and M_1 respectively; the region outside of S is source-free. The current sources within S produce electric fields E_1 and magnetic fields H_1 everywhere. The equivalence principle allows the sources lying inside the volume V_1, to be replaced by equivalent fields which will generate the same fields external to the surface S.

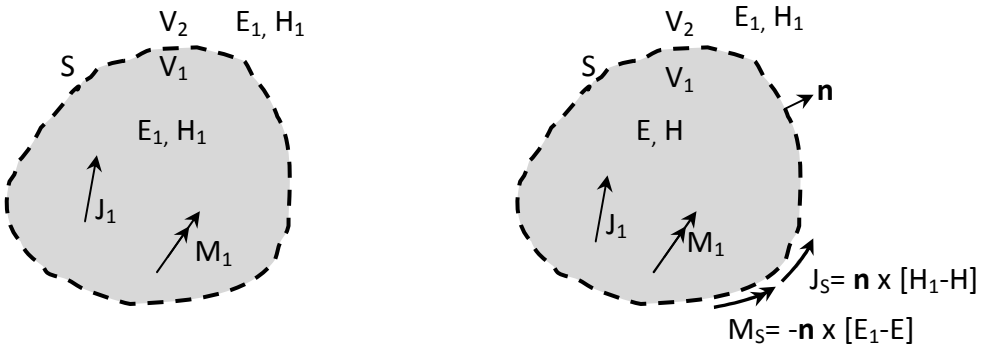

(a)Actual Problem (b) Equivalent Problem

Figure 2.7 - Illustration of Field Equivalence Principle for an Arbitrary Surface.

To accomplish this, the actual sources J_1 and M_1 are removed and an arbitrary E and H field is assumed to exist within V_1, while E_1 and H_1 still remain in V_2. For the two fields to exist on each side of the boundary S, two equivalent current sources J_S and M_S

$$J_s = \hat{n} \times [H_1 - H] \quad \text{on } S \tag{5}$$

must satisfy the boundary conditions of the tangential electric and magnetic field components [1] where

$$M_s = \hat{n} \times [E_1 - E] \quad \text{on } S \tag{6}$$

The surface currents are assumed to be radiating into an unbounded medium and will produce equivalent fields E_1 and H_1 only external to S. Internal to S, the tangential components of the E and H fields are only required to solve for the surface currents J_S

and M_S, but are arbitrary and inconsequential nonetheless. Love's Equivalence principle further simplifies this approximation by assuming that there is a null field within *S*, with only perfect conductors (electric or magnetic). Then, E and *H* inside of *S* are identically zero and the surface currents will only produce electric and magnetic fields outside of *S*. The equivalent currents will then be reduced to:

$$J_s = \hat{n} \times [H_1 - H]\,|_{H=0} = \hat{n} \times H_1 \quad (7)$$

$$M_s = -\hat{n} \times [E_1 - E]\,|_{E=0} = \hat{n} \times E_1 \quad (8)$$

The above outlines techniques for solving the radiating fields from an arbitrary surface. The field solutions are valid for both near-field and far-field regions external to the surface *S* [1]. The ADS Momentum solver relies heavily on these principles and approximations to implement the Method of Moments for the slot structures experimented with here.

2.5 Motivation for Using a CPW-fed Slot Antenna

Various feeding techniques like stripline, microstrip and CPW are available for the slot [25]. Stripline, however, is often undesirable because its complex structure makes it more difficult to manufacture than microstrip and CPW. Stripline is also prone to higher-order propagation modes.

Microstrip feeds work by coupling energy from the backside of the substrate, through the dielectric. In its simplest form, the feed line, usually of 50Ω characteristic impedance, is a conducting strip that lies perpendicular to and centered on the slot it

excites. The strip can be electrically shorted through the dielectric to the slot's edges (Figure 2.9). Alternatively, the microstrip can be terminated in an open-circuited stub by extending the microstrip feed beyond the slot a quarter-wavelength, effectively shorting the line to the slot (Figure 2.10).

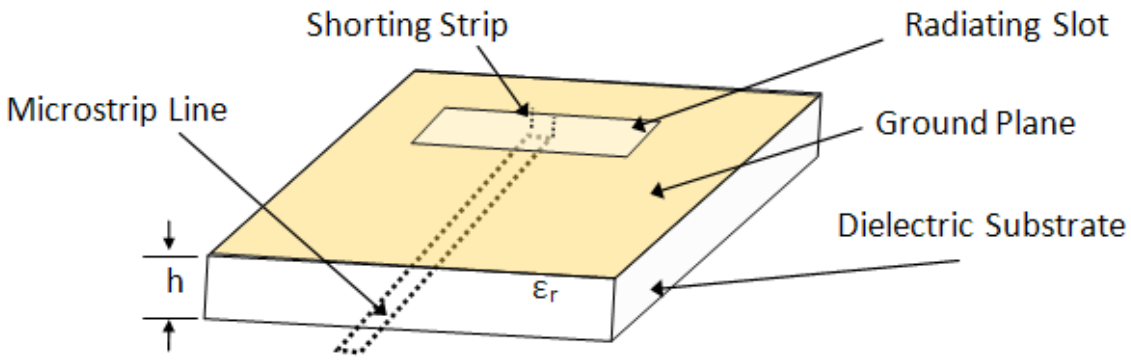

Figure 2.8 - Slot Excited by Shorted Microstrip Feed.

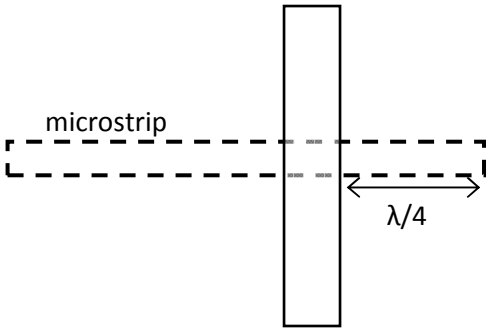

Figure 2.9 - Slot Excited by Effectively Shorted Microstrip Feed.

The impedance presented by the slot, as seen by the microstrip feedline, may not be evenly matched, resulting in reflections, power loss and reduced efficiency. As compiled in Bhartia, Bahl, et al, the input impedance of the slot can be adjusted with three different techniques.

1. The microstrip feed can be placed off-center 2.11(a)

2. The slot can remain center-fed but tilted from orthogonal 2.11(b).
3. The feed can be reactively loaded by extending or shortening the microstrip line 2.11(c).

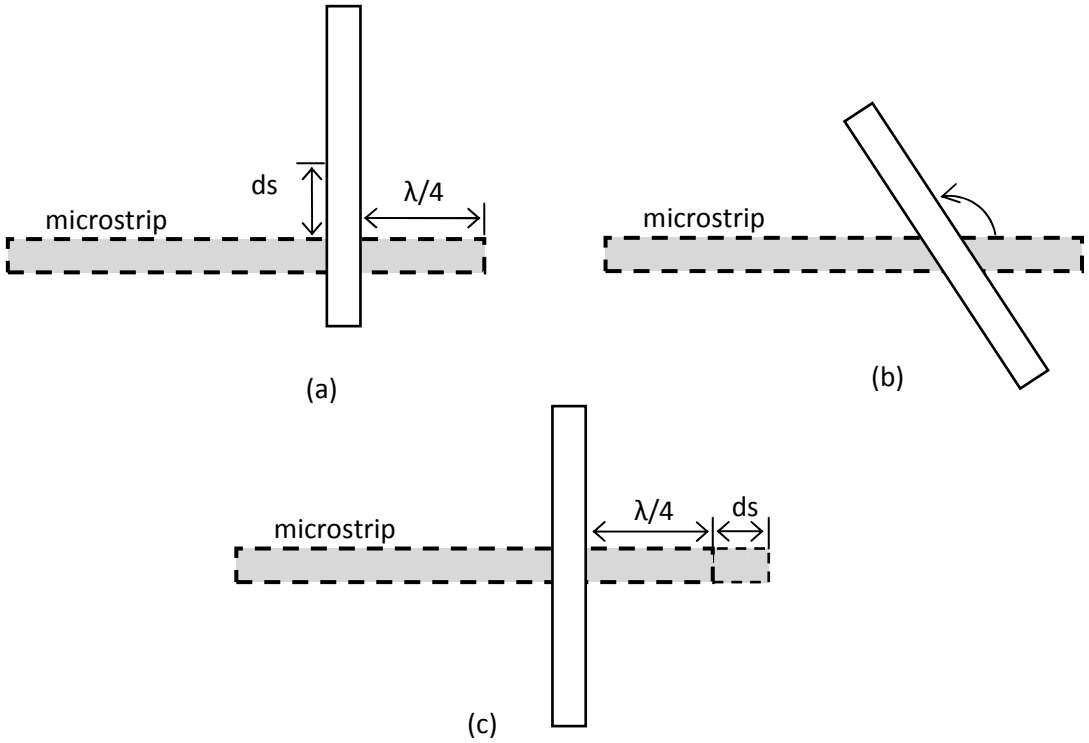

Figure 2.10 - Various Microstrip Feeding Techniques for the Slot.

While very common still, microstrip feeds require processing to be done on, at least, two metal layers. Subsequently, these layers must be accurately aligned during post-processing to function effectively. With CPW, the signal and ground lines share the metal conductor plane, atop the dielectric material. The simplicity of this feeding technique is a natural choice for the slot because the slot and the feed share the same metal layer and can be processed simultaneously. CPW feeds are also known to have lower radiation leakage and less dispersion than microstrip lines [19]. Although it will

not be exercised here, CPW feeds also facilitate the parallel and series-connection of mounted (both active and passive) components, thereby eliminating the need for vias.

There are a multitude of CPW feed techniques available for the planar slot antenna. A major issue concerning a CPW feed is the need for a suitable transition between it and the slot. Originally proposed by Nesic [10] 2.12(a), a center-fed, wavelength long slot may be the most straightforward. Current travels down the CPW feed and, upon reaching the slot, has two paths of equal impedance presented by the two slot portions. Upon its return to ground, the current is equally split and creates a radiating E-field across the slot as it moves along the edges. An off-set CPW feed (Figure 2.12(b)) can be used in a similar manner to the microstrip off-set for proper impedance matching of a full-wavelength long slot. Finally, a capacitively-fed slot in Figure 2.12(c) and inductively-coupled slot Figure 2.12(d), each a half-wavelength long, serve as viable alternatives.

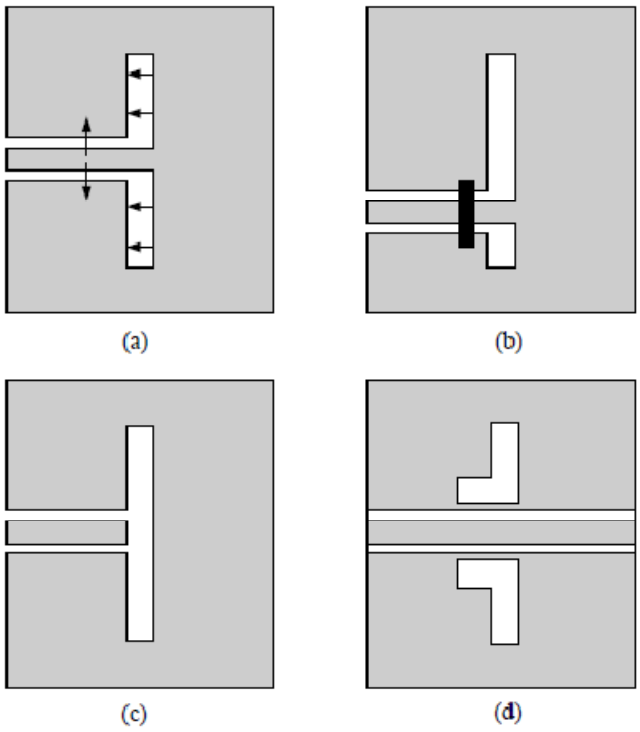

Figure 2.11 - CPW-fed Slot Antennas.

A downside of the CPW feed is its susceptibility to voltage difference between the two sides of the ground plane. To prevent this from occurring, air bridges are sometimes used to electrically tie the two ground planes together.

2.6 Slot and Dipole Relations

Dipole antennas are readily understood and analyzed. For this reason, the slot antenna is commonly characterized in terms of its dipole-like behavior [27]. There has been much done in the endeavor of formulating these slot-dipole relations. Originally derived for applications in optics, Babinet's principle describes how any field produced by an EM wave passing through an arbitrary aperture in a metal screen will effectively produce the same radiated pattern as the printed dipole which would perfectly fill that

opening. Shown in Figure 2.13, if the metal sheet around the slot is of infinite extent, the radiated fields can be considered virtually identical except that the electric and magnetic field vectors are orthogonally interchanged [28]. An additional consequence of the E- and H- vector orthogonality is that their respective polarizations are also known to be orthogonally related. The dipole radiates an E-field which aligns in the direction of its length. The E-field radiated by the slot, meanwhile, is perpendicular to its length.

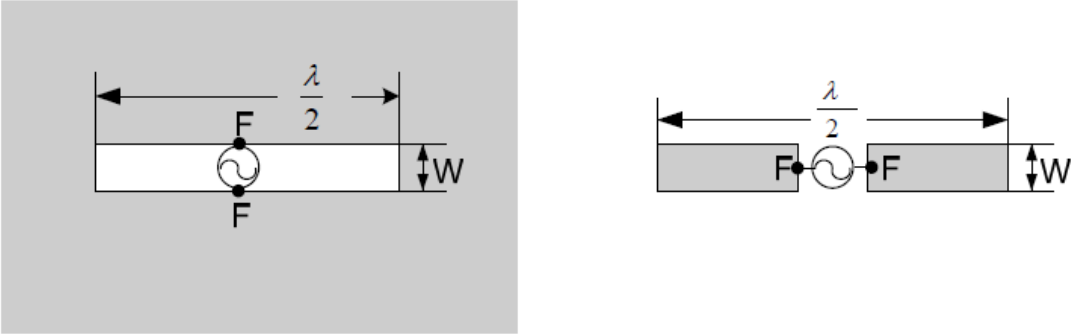

Figure 2.12 – Slot (a) and Dipole Complement (b).

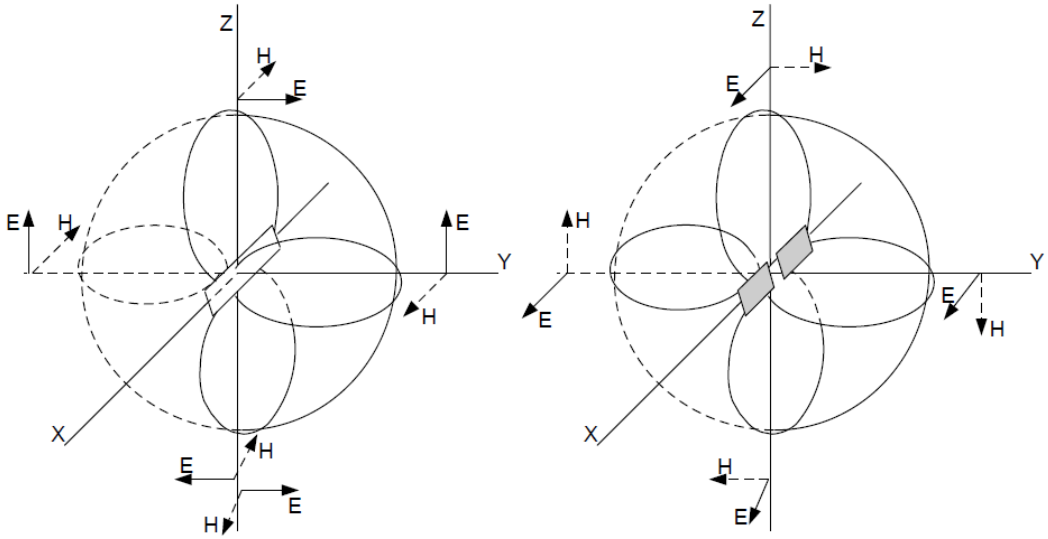

Figure 2.13 – Radiated fields from Slot in an Infinite Ground Plane (a) and Radiated Fields from Complimentary Dipole.

This fact could be exploited in any design process. The time it takes for the Momentum solver to produce a solution for the given geometry is directly related to its planar footprint and solution frequency. The area required to physically describe the printed dipole is much reduced, relative to the equivalent slot and, therefore, requires much less time to be solved for. Many principles and solutions that apply to dipoles can also yield insight to the slot behavior.

2.7 Chapter Summary and Conclusions

Slot antennas have been continually explored and developed in the last six decades and still continue to be an active area research today. Their planar form and simple but robust structure makes them desirable in a wide range of communication applications. Also, the slot's ease of fabrication, ability to be integrated with other electronic components and wide operating bandwidths gives the slot, in some instances, an advantage over patch radiators. The collection of works cited here have shown that the CPW line is a natural feed candidate for slot antennas and can effectively feed an array of slot elements. This work will pursue the development of the center-fed, wavelength-long slot in the following chapter.

CHAPTER 3

THE SINGLE CPW-FED SLOT ELEMENT

3.1 Introduction

In this chapter, the CPW center-fed, rectangular slot antenna is introduced. The individual slot element, while simple, is the basis of the four-element array investigated in this work and must be fully constructed, characterized and understood before the array can be further developed. The CPW-fed slot, by definition, is an intentionally-leaky, uni-planar structure. The slot antenna can be easily fabricated with conventional PCB processes. With the backside copper-cladding removed in its entirety from the PCB substrate, the slot element is formed by etching or milling away some pattern of copper-cladding on the top metallic layer (Figure 3.1).

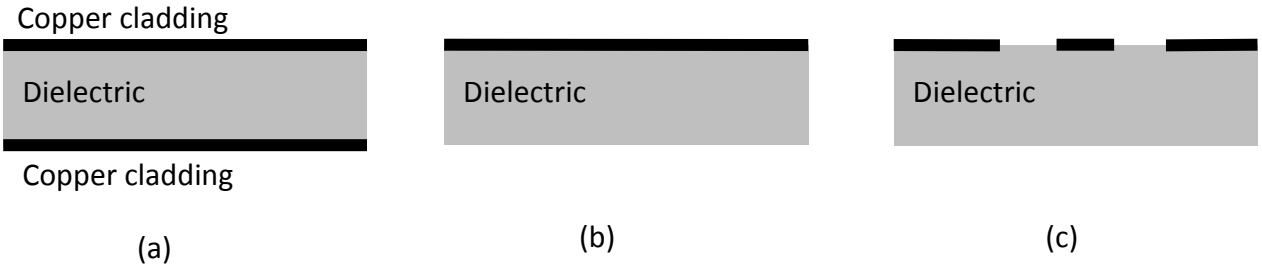

Figure 3.1 - Standard PCB (a), PCB with Backside Copper Removed (b), Slot Geometry Formed in Top Metallic Layer of PCB (c).

There has been a substantial amount of work in the investigation of complex slot geometries to achieve, among other things, compact sizes and extremely wide bandwidths. However, the single slot element is not the focus of this work. The individual slot geometry was intentionally kept simple with only a few adjustable dimensions so that it may be easily expanded into a linear array. To this end, a rectangular, center-fed slot was chosen for this project. Its width and length can be adjusted to precisely set the resonant frequency and match impedance to the driving port. Bow-tie slots could also be a substitute for the rectangular slot and were given brief attention. Agilent's ADS and Momentum software were used throughout the design process to construct, simulate and analyze the slot. A combination of simulated and measured results for return loss and radiation pattern will be given here.

3.2 Slot Length

As given in Chapter 2.5, Babinet's principal illustrates that the electric and magnetic fields for the printed slot and complementary printed dipole and are orthogonally equivalent. On that premise, the current distribution for a dipole is equal to and interchangeable with the voltage distribution along the edges of the slot. The slot is long enough that its current and voltage distribution is not uniform along its length. Therefore, adjustments in the length of the CPW slot will setup the boundary conditions and determine how the voltage and current distribute along the metal surrounding the slot. Ultimately, this distribution will establish the resonant frequency of the slot.

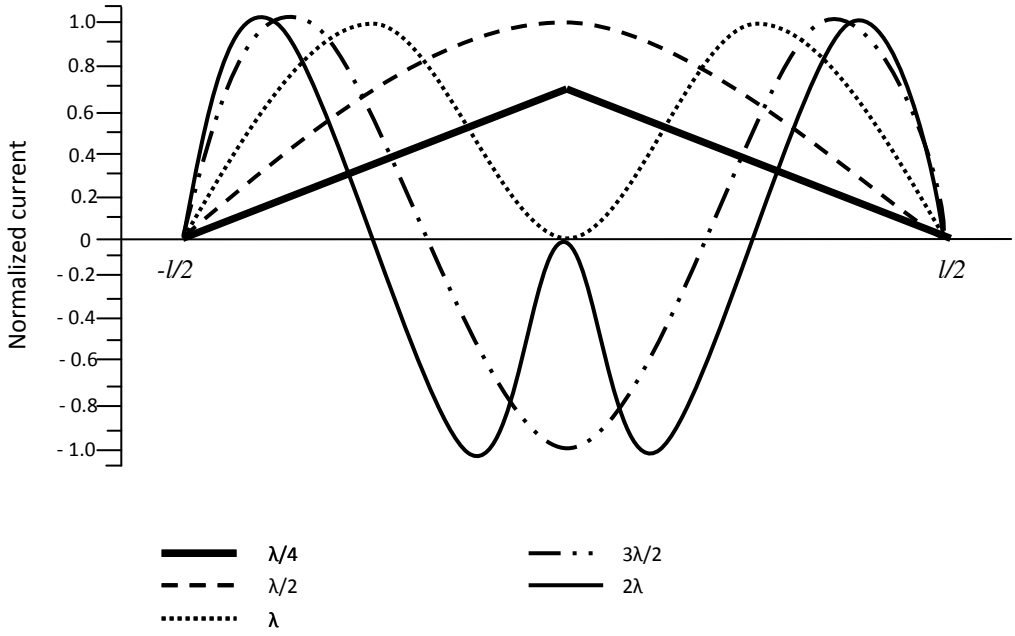

Figure 3.2 - Standing Current Distribution for Dipoles.

Much like its dipole counterpart, the slot length will resonate at the common wavelength dimensions or multiples thereof. At resonance, dipoles of these discrete lengths will produce standing wave patterns, a depiction of the current or voltage distribution along their lengths. Figure 3.2 illustrates the normalized standing current wave for dipoles of various lengths. These standing current waves for the dipole are identical to the standing voltage waves of the slot, where a current peak on the dipole correlates to a voltage peak across the slot.

The length of the slot explored in this work was set at a full wavelength (λ_g) and is center-fed, as proposed by Nesic [10]. Conceptually, the lowest impedance of the full wavelength-long, center-fed slot occurs at the feed (the slot's center) and at the slot's ends. Because the metal surrounding the slot is considered to be perfectly conducting,

the electric field tangential to the slot is taken to be zero. Therefore, at the slot's center and ends, the impedance is at its lowest and current at its maximum. With no resistance at the end of the slot, the voltage there is near zero and grows until it reaches its maximum, a point one quarter-wavelength from the end of the slot. For a given center frequency, the slot length of one wavelength could roughly be determined by:

$$\lambda_g = \frac{c}{f_c \cdot \sqrt{\epsilon_{eff}}} \tag{9}$$

where λ_g is the guided wavelength, f_c is the center frequency of resonance, c is the speed of light and ε_{eff} is the effective permittivity surrounding the transmitted signal. The precise length, then, was determined empirically through simulations in ADS.

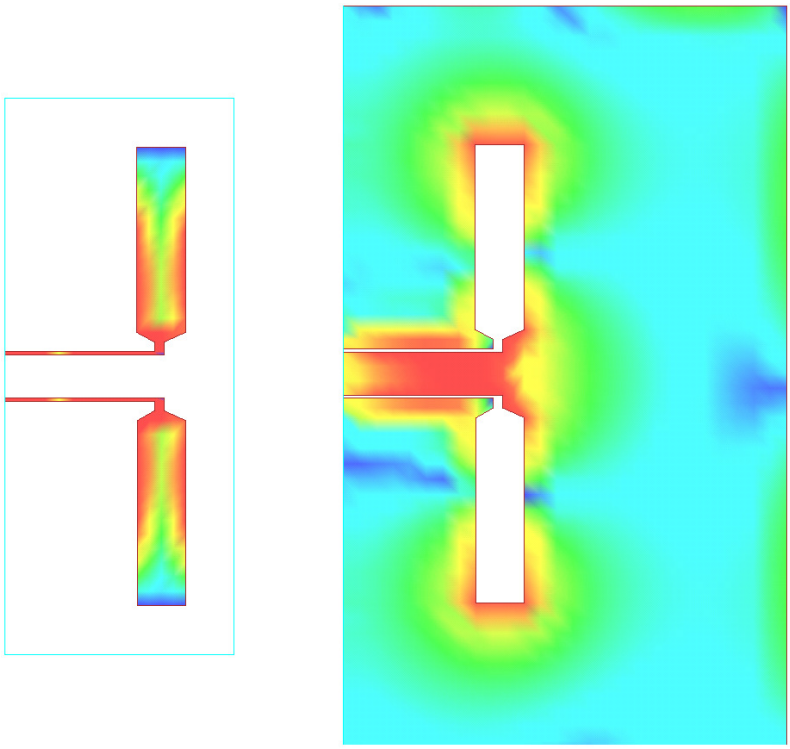

(a) (b)

Figure 3.3 - Simulated Current Distribution for a CPS-fed Printed Dipole (a) and CPW-fed Slot (b).

Figure 3.3(a) shows the current distribution for a matched, wavelength-long, printed dipole. The current behaves as predicted, closely corresponding to the curves depicted in Figure 3.2. The densest current accumulates along the center of the two slot segments. Current density falls off gradually as it gets closer to the end where it eventually vanishes. Conversely, the current distribution for a printed slot antenna is shown in Figure 3.3(b). The current for the slot is inverted from that of the dipole and is distributed throughout the finite metal sheet surrounding it. It is somewhat incidental to show how the current distribution aligns with the expected model; however, it is a powerful means of determining whether the elements in the subsequent series-fed array are operating in-phase. When fed in-phase, current will synchronously rise and fall on the slots' edges; this will be apparent by plotting the current distribution.

The overall length of the slot, end to end, is not simply a function of the radiating section of the slot, but is also a factor of the feed and taper dimensions. To focus on the effects caused by the radiating, rectangular aperture, the slot length, for these purposes, will be with respect to the dimension *l* in Figure 3.4(a). Feed and taper effects will be addressed in subsequent sections.

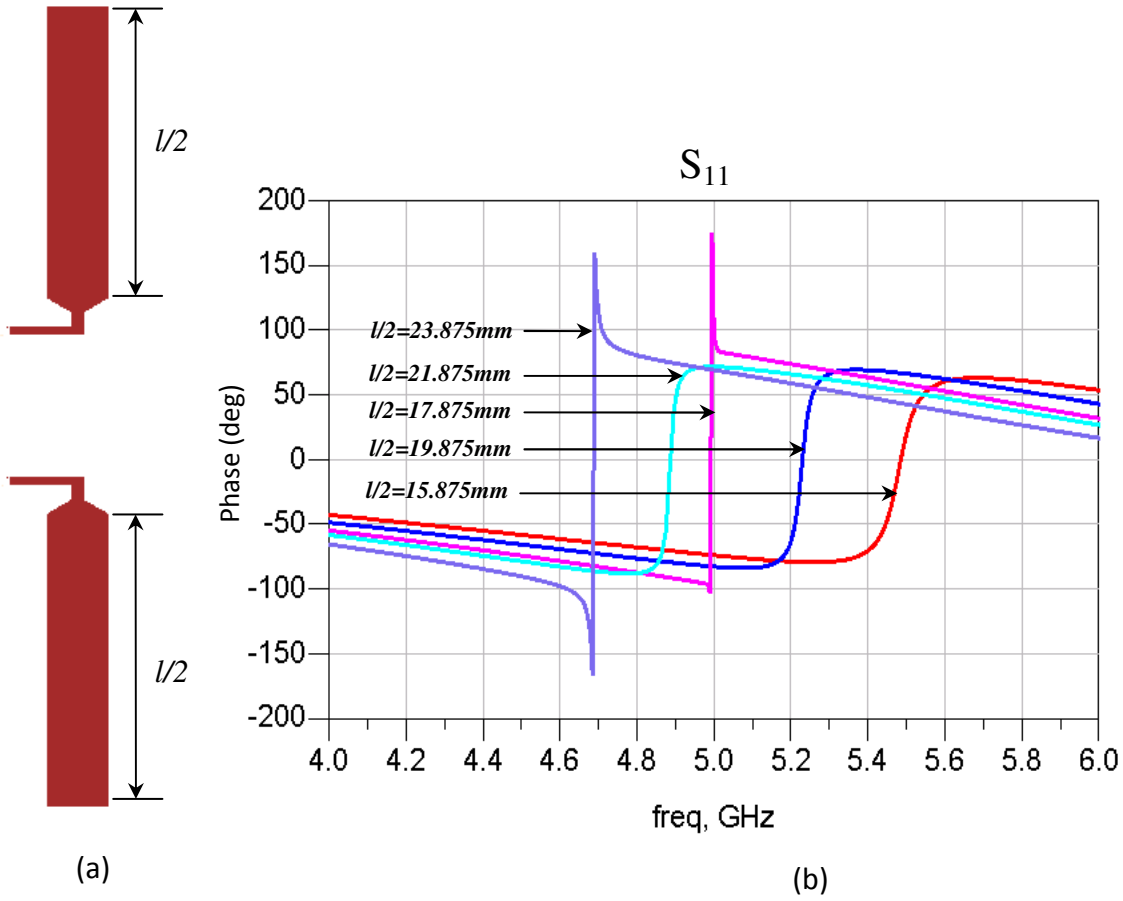

Figure 3.4 – Slot Length Adjusted (a) and Simulated Frequency Shifts (b).

The curves of Figure 3.4 depict how variations in the slot lengths translate into shifts in the center frequency of resonance. A zero-crossing in the phase of S_{11} is indicative of resonance; the slot can be set to resonate at nearly any frequency by adjusting its length. It was noted that a 10% variation in the slot length (l) corresponds to a shift of about 9.44% in the center, resonant frequency.

3.3 Feed Effects

The current and/or voltage distributions given in Figure 3.2 are ideal in the sense that they are based on an ideal feed that does not disturb the field distribution. When a practical feed is introduced, however, some perturbations occur, forcing the fields to arrange differently. The impedance of the device, then, is altered accordingly, if only slightly.

Most close-form expressions for antenna analysis assumes the feed gap(*s*) for conventional dipole antennas (Figure 3.5) to be negligible, if not identically zero. To account for feed effects of a real feed, the current distribution of a simple dipole can be altered to include an additional, "quadrature term" [1]. Equations 10 and 11 include the term, preceded by the coefficient (*p*), which factors in the feed radius (equivalent to slot width) and feed gap (equivalent to CPW signal width). The value of *p* decreases as these dimensions become smaller, thus reducing the weight of the second term.

$$I_e(x',y',z') = I_0\left\{sin\left[k\left(\frac{l}{2}-z'\right)\right] + jpI_0\left[\cos(kz') - \cos\left(\frac{k}{2}l\right)\right]\right\} \quad for\ 0 \le z' \le l/2 \tag{10}$$

$$I_e(x',y',z') = I_0\left\{sin\left[k\left(\frac{l}{2}+z'\right)\right] + jpI_0\left[\cos(kz') - \cos\left(\frac{k}{2}l\right)\right]\right\} \quad for\ -l/2 \le z' \le 0 \tag{11}$$

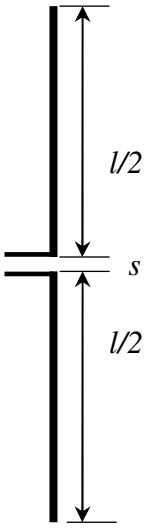

Figure 3.5 - Conventional Dipole with Gap Feed Included.

Equations 10 and 11 are merely approximate methods of determining how current distributions are disrupted by the feed. To accurately determine these effects, a numerical technique, like MOM, must be employed. Figure 3.6 relates the influence signal width and slot width have on the slot performance.

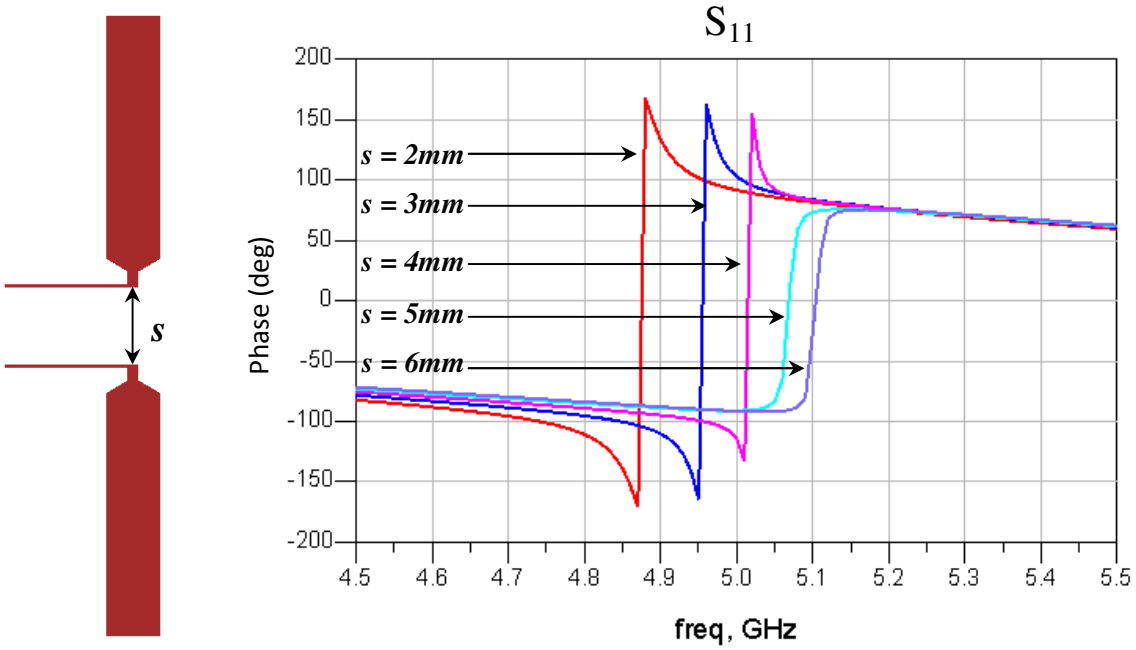

Figure 3.6 – Simulated Signal Widths Effects on Slot Performance.

Signal width has a direct and apparent effect on the frequency of resonance. The effect is similar to what would be expected for a dipole. An increase of 1mm in signal width increases the resonant frequency by ~ 75MHz.

3.4 Slot Width

While the slot length, taper and feed will set the boundary conditions and, in turn, the frequency of resonance, the width of the slot dominantly controls the impedance of the slot. By increasing or decreasing slot width, the resulting capacitance formed by the electric field across the slot is proportionally and respectively lowered or raised. This capacitance directly controls the slot's input impedance and increase when the width is increased. Similarly, decreasing slot width will lower input impedance. Thus, slot width can be tuned to match the slot element to the driving source.

Figure 3.7 shows how adjustments in the width of the slot can be better matched to the source for a deeper and wider resonance. A slot was designed with the proper length to resonate at a center frequency of 5GHz. Its width was adjusted to match the 50Ω port driving it.

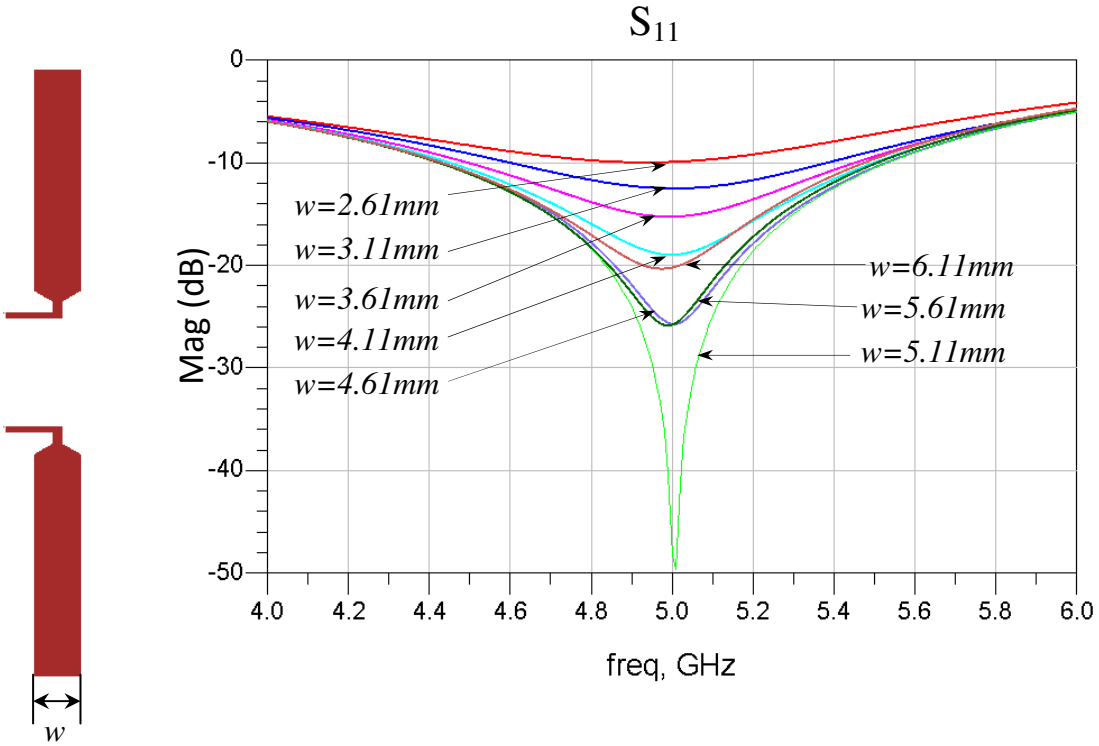

Figure 3.7 – Return Loss Effects of Altering Slot Width.

For the given feed dimensions and slot length, the slot has a width which will be best matched to the source impedance. Away from that width, the match and slot performance will be proportionally degraded due to mismatches and reflections. Precise slot width, too, was determined experimentally in simulations. The narrow slot of 2.61mm (6.5% λg) was not resonating well (with a return loss < 10dB). But, as the slot was incrementally widened, its impedance increased and approached that of the driving port and energy began to couple more effectively into the device. The 5.11mm (12.84% $\lambda_{g)}$ wide slot was matched almost perfectly where almost all of the inserted power is

being radiated from the element. Beyond 5.11mm, additional increases in slot width caused the slot performance to degrade again, and at a similar rate.

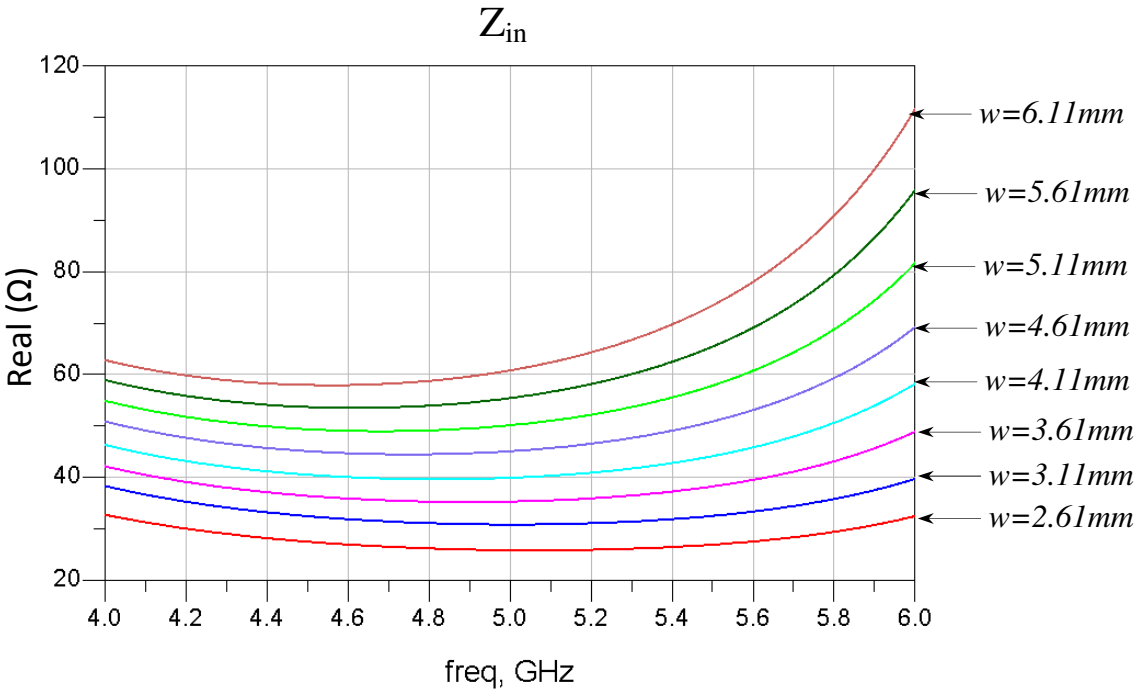

Figure 3.8 - Input Impedance vs. Slot Width.

Inspecting the real input impedance directly gives a good depiction as to how slot width will control the input impedance. At 5GHz, a narrow slot of 2.61mm will produce a relatively stable input impedance of ~25Ω across the entire 2 GHz band. Each half millimeter increase in width returns ~5 Ω of impedance at the ports.

3.5 Taper

Throughout the design process, the slot width was continually adjusted for impedance matching. When the slot parameters are varied, the slot width must be appropriately adjusted to match its impedance to that of the port. If the feed of the slot

is taken to be where the CPW feed line and the slots intersects, it can be seen that by altering the slot width, the feed point of the slot is also shifted. In order to isolate these effects, the feed of the slot (at its center) was given a taper, allowing the slot width to be modified independent of other physical parameters.

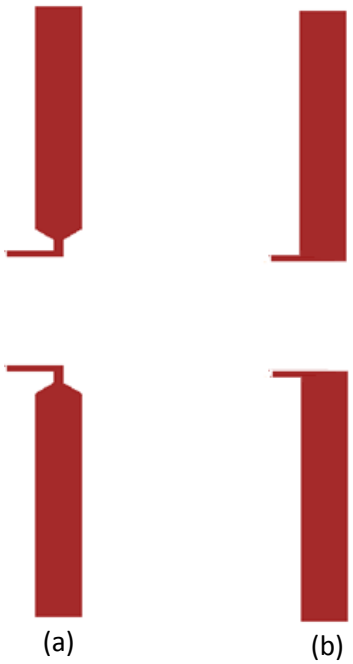

Figure 3.9 – Tapered (a) and Non-Tapered (b) Slot.

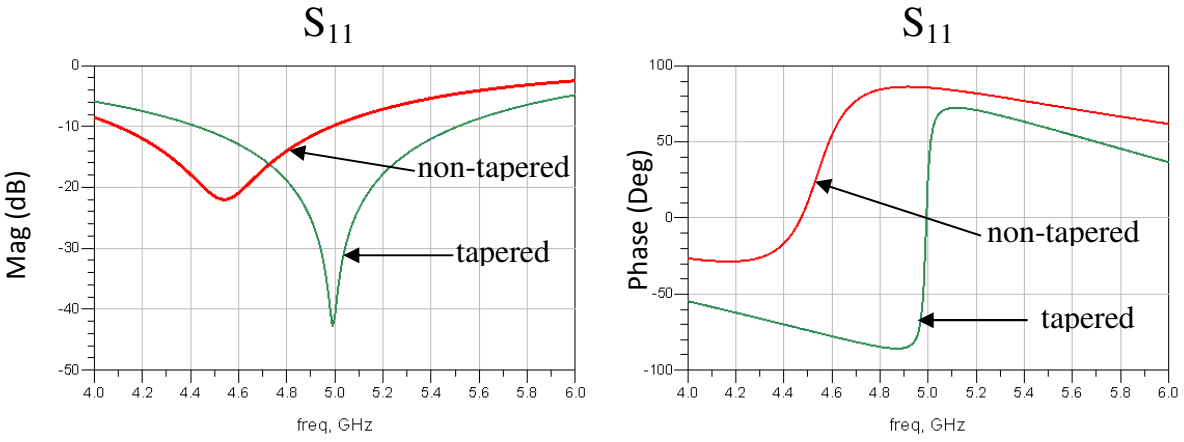

Figure 3.10 – Tapered (green) vs. Non-Tapered (red) Slot.

The effect of the taper is shown in Figure 3.10. Two slots of identical, overall length, width and feeds, differ only by the taper at their base (Figure 3.9). The tapered, rectangular slot radiates near 5GHz. Without the taper, there is an apparent shift of ~500MHz (10%) in the resonant frequency; the slot without a taper is radiating near 4.5GHz. The taper was 2mm or about 4.3% of the total slot length, and was intentionally kept small relative to the size of the slot in order to minimize its effect. The taper shortens the effective length of the slot by reducing the area where current can setup along it edges and adequately radiate across its width.

3.6 Slot Characteristics

3.6.1 Input Impedance

The input impedance of any antenna has an important role in the design process. Indeed, antennas will radiate well and have wide bandwidths strictly because the input impedance they produce is closely matched to the impedance of the port driving them. The slot has complex impedance, composed of both a resistive and reactive component. The total impedance has many contributions including: the impedance mismatches and reflections due to transitions and turns, dielectric losses, impedance shifts from the feed and radiation resistance. The power lost through radiation (R_r) appears as an ohmic loss and can be considered as such in determining the total impedance presented by the antenna. All other losses are generally lumped together into a term R_L. Then, the impedance of the antenna is given by (12)

$$R_A = R_r + R_L$$

where:

$R_r = radiation\ resistance\ of\ the\ antenna$

$R_L = loss\ resistance\ of\ the\ antenna$

That is, the total real resistance at the driving port R_A is the resistance due to radiation and all additional losses of the antenna. It is desired that the bulk of the input impedance be the resistance due to radiation, for the losses to be minimized. An ideal antenna would be lossless, in which case, the input impedance at resonance is identical to the radiation resistance. Efficiency is a figure of merit which demonstrates the antenna's ability to radiate and is directly derived from the input resistance. Efficiency, is given as

$$e_{cd} = \frac{R_r}{R_r + R_L} \tag{13}$$

and shows that as all other losses tend to zero, the antenna efficiency will become 100%. Conversely, as the losses increase for a matched antenna, the efficiency will drop, consequentially reducing the amount of input power which is being properly radiated.

The slot is said to be resonating when the input impedance becomes purely real, or the reactive component goes to zero. This behavior can be observed readily when the imaginary part of the return loss (S_{11}) has a zero-crossing. Even though the impedance of the slot may be purely real, it may not be radiating well if it is not properly matched to its driving source. The antenna is said to be radiating well when the magnitude of the return loss is greater than 10dB ($S_{11} \leq$ -10dB). In order for energy to be properly coupled into the device and minimize reflections (maximize power transfer), it is important for the slot

and source to be impedance matched. Consequently, poorly matched elements will result in low gain and low efficiency.

3.6.2 Radiation Pattern

When properly matched, the slot will have the ability to take the electrical signal from the driving source and effectively transform it into a transmitted EM wave. A well-matched slot was simulated in Momentum and its 3-D radiation pattern plotted at the center frequency. In Figure 3.11, a single radiating slot produces the typical "doughnut" radiation pattern that is nearly identical to that of its complementary dipole. This fact remains despite the presence of the large, metal sheet surrounding the slot. The electric field intensity can exist near the surface of the conducting plane because the electric fields lines are perpendicular to the surface. The electric fields, however, cannot occupy the plane itself, causing a thinly sliced negation or perturbation in the 3-D pattern [28]. Poynting's vector is used to determine the pattern of radiated power and dictates that the dipole and slot do not radiate power evenly in all directions; they are anisotropic by nature. For these elements, radiation is at a maximum at broadside and rapidly decays in the direction of the slot's ends.

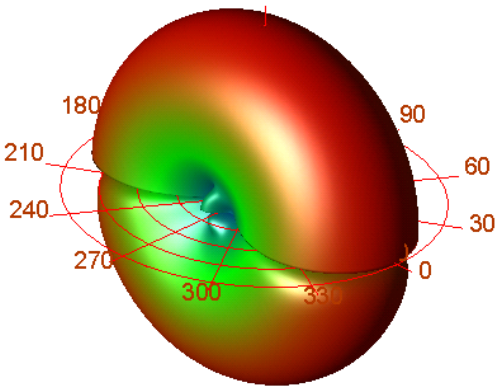

Figure 3.11 - Radiated Pattern of Center-fed, Wavelength-long Slot with No Reflector.

Still, the end goal for this work is to produce a single, directive, uni-directional major lobe. Without a reflector, the single slot has directivity of 3.826 dBi. To redirect or regain power that would otherwise be lost through backside radiation, a flat, metallic reflector can be placed behind the slot at a conventional distance of one quarter-wavelength (λ/4). A slot with a finite reflector is shown in Figure 3.12(a).

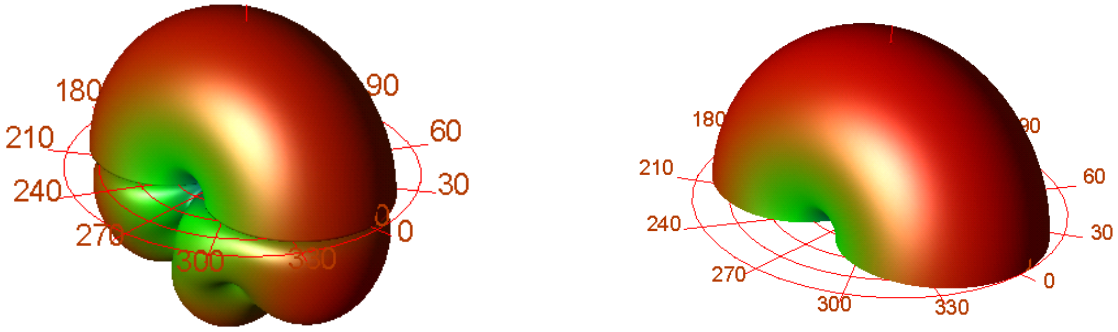

Figure 3.12 - Radiated Pattern of Center-fed, Wavelength-long Slot with Finite Reflector (a), and Infinite reflector (b).

The arrangement will partially suppress backside radiation and increase directivity to 4.841 dBi. To fully capture all backside radiation, a reflector of infinite size would be necessary but is nevertheless impractical. Figure 3.12(b) shows the half-doughnut pattern, a theoretical consequence of an infinite reflector placed behind the slot. The pattern has virtually zero backside radiation with an improved directivity of 6.313dBi.

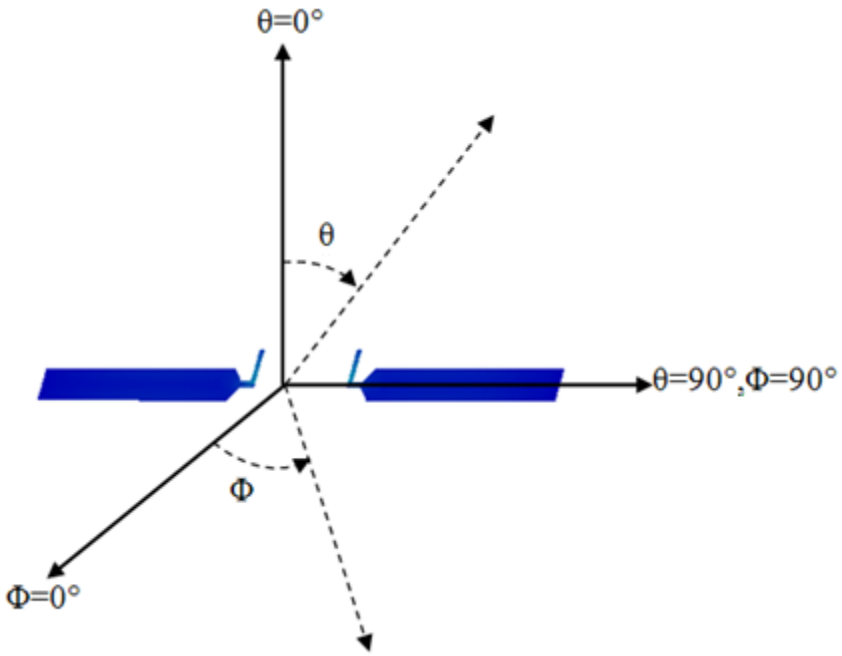

Figure 3.13 - Spherical Coordinate System for Slot Simulation.

The length of the slot is directly related to its 3-dB beamwidth. The 3dB beamwidth, or half-power beamwidth (HPBW), is a figure of merit for the major lobe of the antenna. The rate at which the intensity falls off is representative of the power density of the beam and describes its ability to focus energy in a given direction. With the slot oriented as shown in Figure 3.13, the 2-D plot of Figure 8 represents a slice of the total radiated field as seen at $\Phi = 0°$, and swept about θ. At broadside ($\theta = 0°, 180°$) the radiation is most intense and gradually reduces, eventually into a null, away from broadside, at the slots' ends.

Table 3.1 - The 3-dB Beamwidth of Common-length Dipoles

$l<<\lambda$	3-dB beamwidth = 90°
$l=\lambda/4$	3-dB beamwidth = 87°
$l=\lambda/2$	3-dB beamwidth = 78°
$l=3\lambda/4$	3-dB beamwidth = 64°
$l=\lambda$	3-dB beamwidth = 47.8°

An antenna can radiate well at many different wavelength proportions, but its half-power beamwidth is established with the length of the device; Balanis [1] presents some for standard-length dipoles in Table 3.1. The table shows that longer dipoles have the narrower beamwidths at broadside.

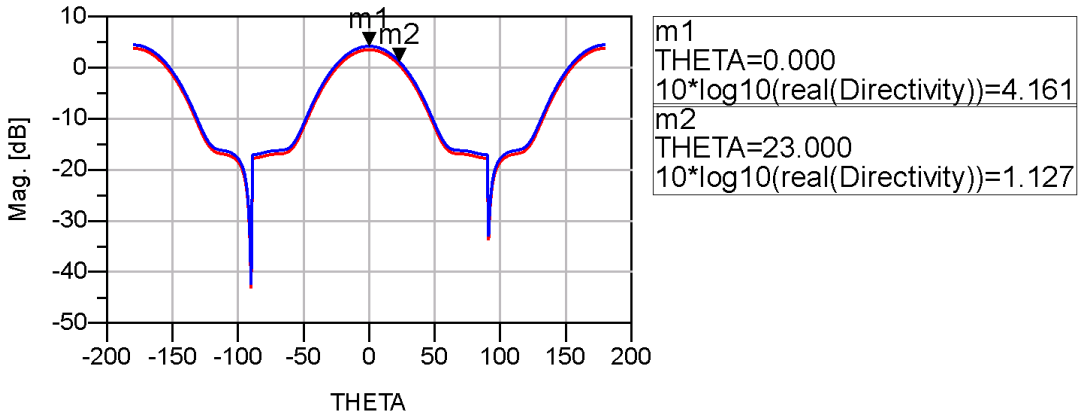

Figure 3.14 – 3-dB Beamwidth for Wavelength-long Slot.

The simulated slot has a half-power beamwidth of about 46°, nearly identical to the mathematical prediction for a wavelength-long dipole in Table 3.1. Wavelength-long slots and dipoles are capable of narrower HPBW than those of shorter lengths. As the

length increases beyond one wavelength ($l > \lambda$), however, the number of sidelobes begins to increase [1].

3.7 Results and Comparison

Based on the design procedures and considerations given above, a rectangular slot was designed and fabricated to operate around 5GHz. Shown in Figure 3.15, the slot was milled into the Rogers 4003C substrate. A coax-to-CPW connector was used to feed the slot and make measurements.

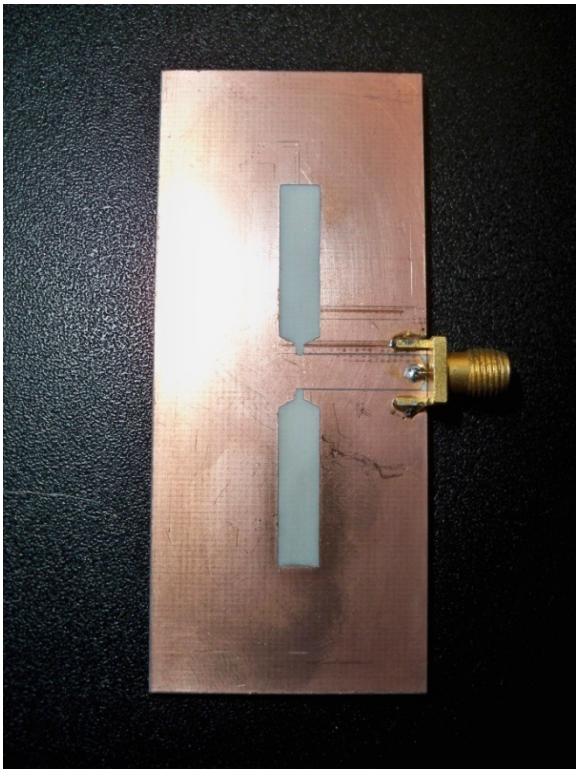

Figure 3.15 – Fabricated Rectangular Slot.

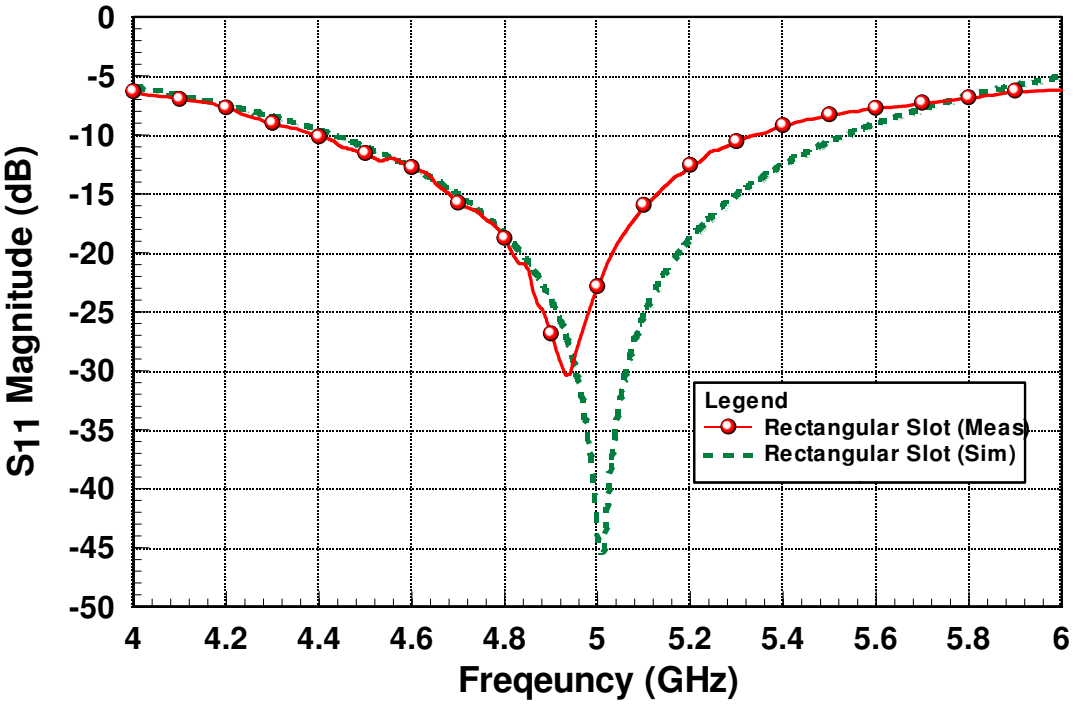

Figure 3.16 – Comparison of Measured vs. Simulated Return Loss for Rectangular Slot.

Figure 3.16 shows the return loss of the measured and simulated rectangular slot. The simulated and fabricated versions behave similarly, but the center frequency of the fabricated slot is slightly off 5GHz and suffers from ~2.3% less BW.

As a viable alternative to the rectangular slot, bow-tie slots were also considered during the design process. Bow-tie slots have been shown to be capable of very wide bandwidths and could be easily incorporated into this array design. The rectangular slots can be flared at their ends like that of Figure 3.17(a) or flared and rounded 3.17(b). In the latter case, the design allows the current to flow around the slot more freely with fewer abrupt turns and transitions, theoretically increasing bandwidth.

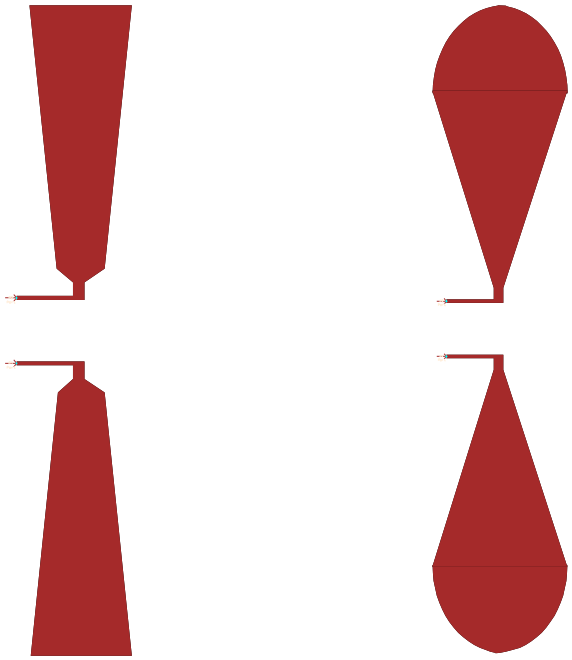

Figure 3.17 - Investigated Bowtie Styles.

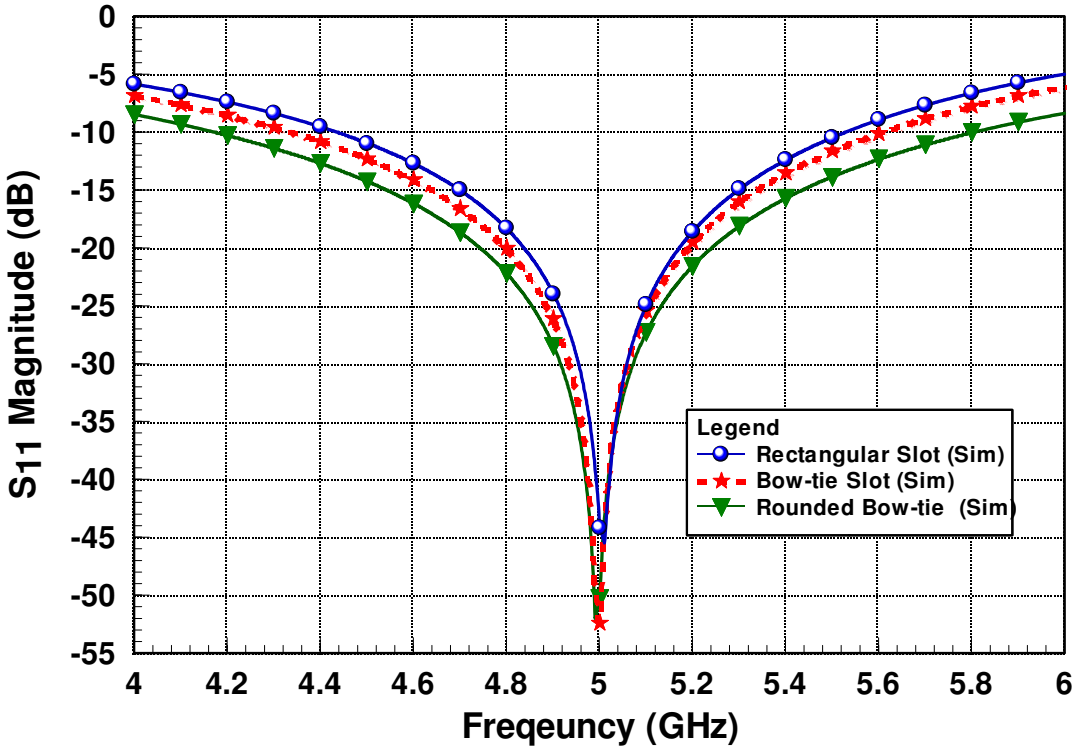

Figure 3.18 – Simulated Return Loss for Three Slots.

The simulated bow-tie slot has a 25.36% bandwidth and the simulated, rounded bow-tie has 32.4%, 4% and 10.8% more respectively than the rectangular slot. Both were fabricated (Figure 3.19) and measured.

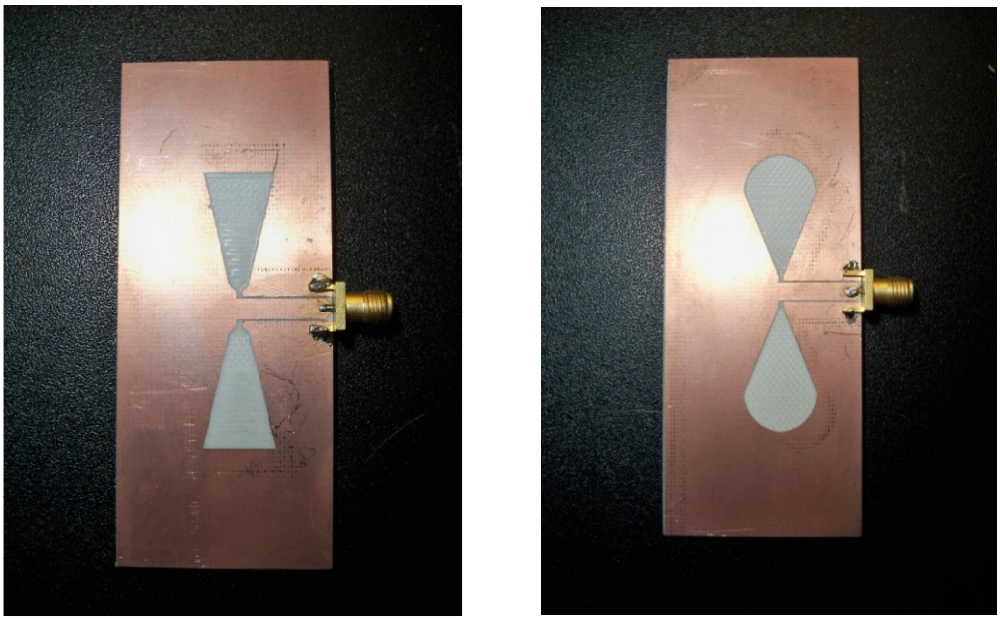

Figure 3.19 – Fabricated Bow-tie Slots.

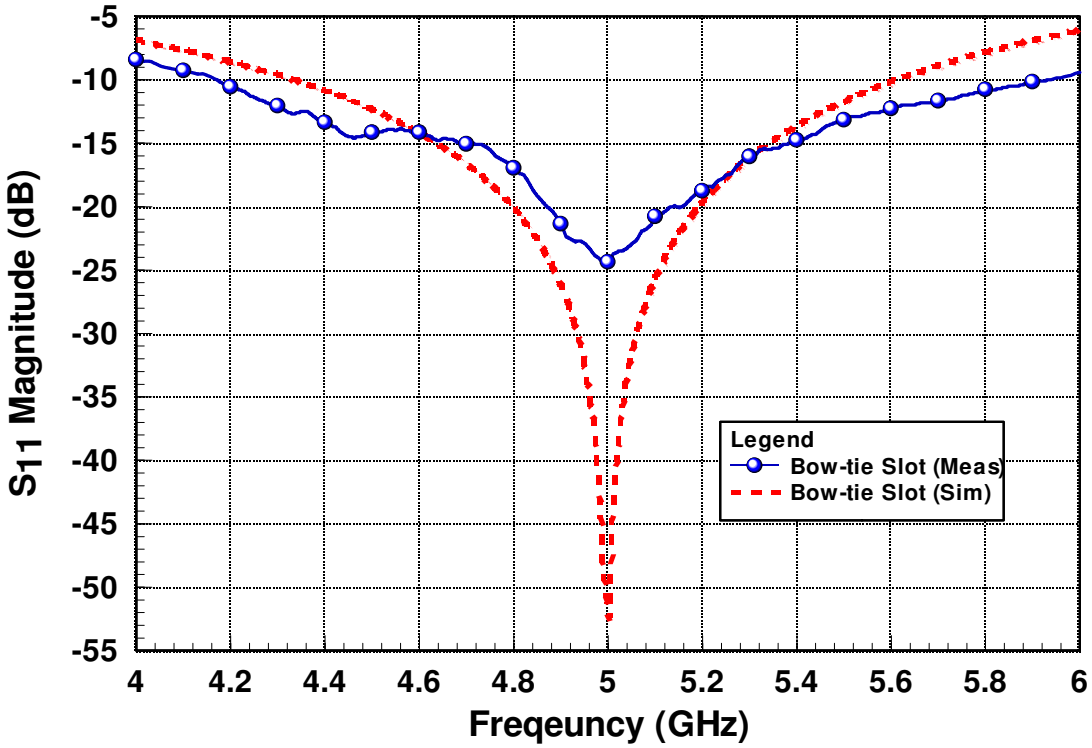

Figure 3.20 – Comparison of Measured vs. Simulated Return Loss for Bow-tie slot.

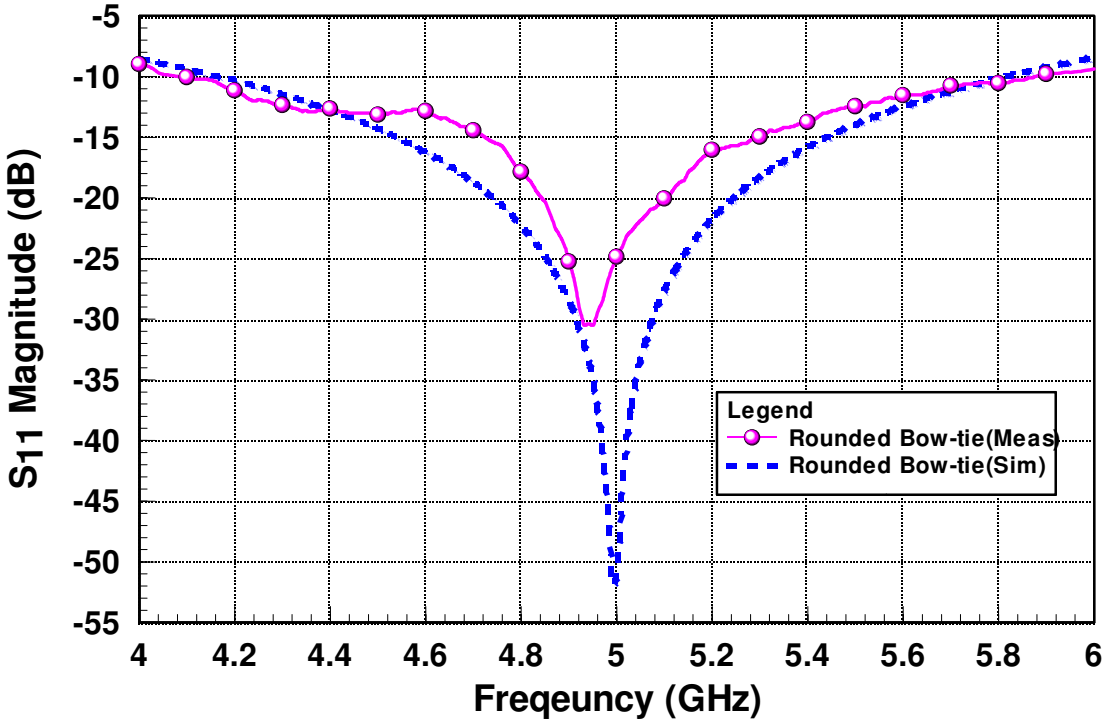

Figure 3.21 – Comparison of Measured vs. Simulated Return Loss for Rounded Bow-tie slot.

Neither of the measured slots have a resonance as deep as their simulated counterpart. Still, both resonate well near the center frequency and have wider bandwidths.

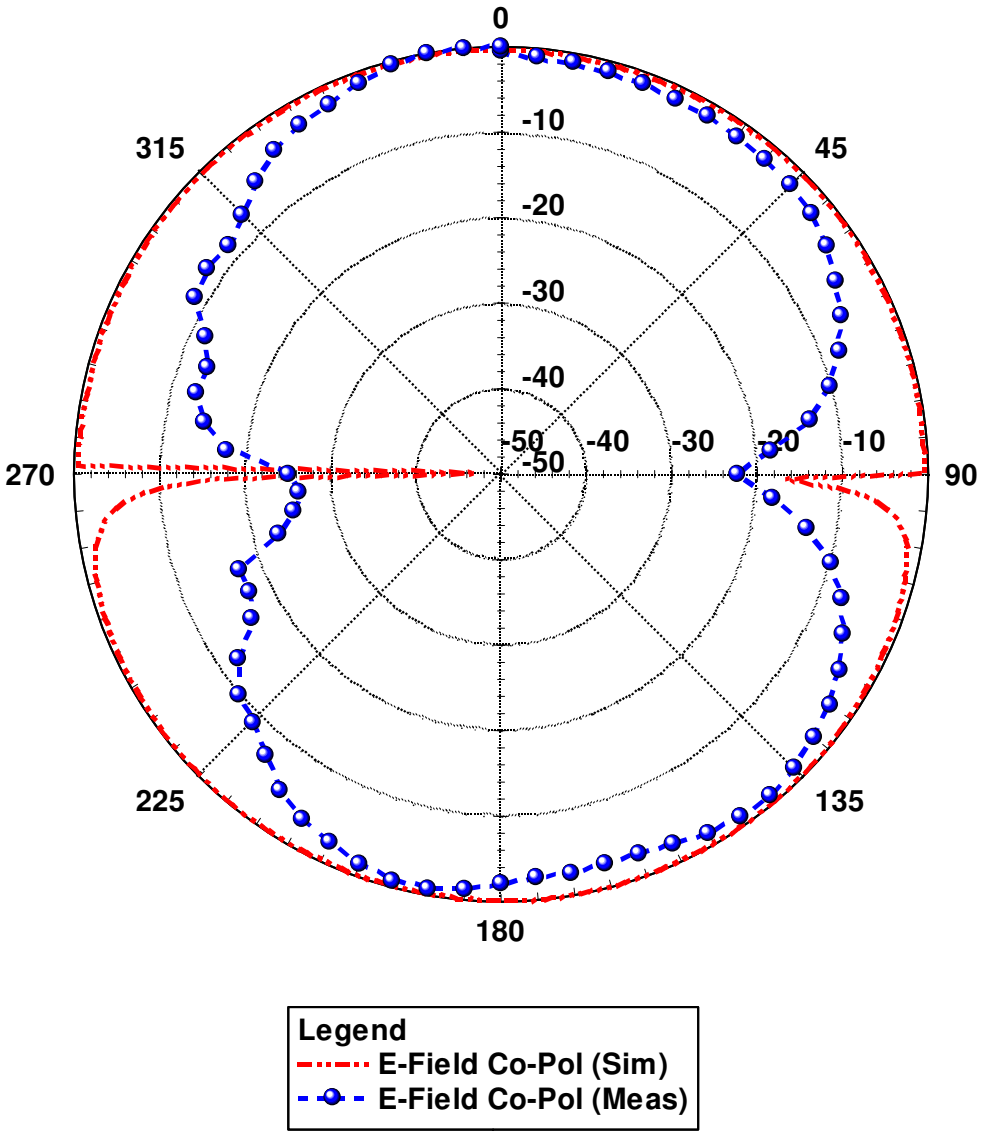

Figure 3.22 –Measured vs. Simulated E-Field Co-polarization Pattern.

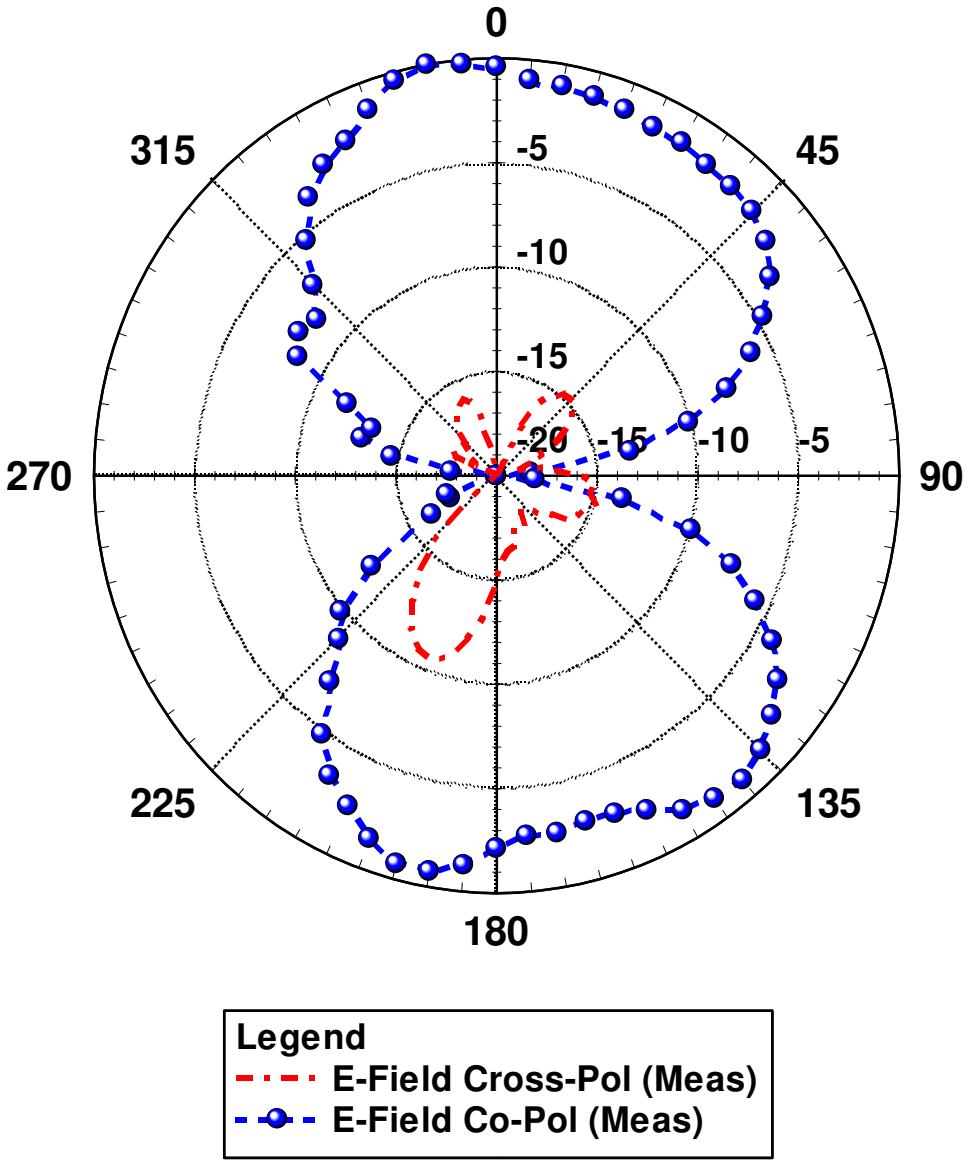

Figure 3.23 –Measured E-Field Co-polarization vs. Measured E-Field Cross-polarization.

3.8 Chapter Summary and Conclusions

A printed, rectangular slot structure was developed, extensively investigated, and shown to be a simple and reliable radiator. The results given here demonstrate that these devices can be made to radiate well by adjusting the slot length, width and feed dimensions. The design process of the slot antenna as described above is straightforward and reproducible for many frequencies and PCB platforms. It does, however, require software-simulated iterations for fine-tuning. A single, rectangular slot can radiate over a >20% bandwidth around 5GHz and additional bandwidth can be attained with bow-tie and rounded bow-tie variations; measured and simulated results closely align. All three will produce a "doughnut" radiation pattern with a relatively narrow beamwidth. A quarter-wave finite reflector positioned behind the slot was shown in simulation to improve the directivity by ~1dB, while an infinite reflector improved directivity by ~2.5dB.

CHAPTER 4

THE FOUR-ELEMENT PLANAR ARRAY

4.1 Introduction

In the previous chapter, the development and characteristics of a single slot antenna were presented. The radiating element could be designed and easily tuned to function over a wide bandwidth. The radiation pattern for the individual element was, however, shown to be very broad, and thus, to have low gain. Many applications, like long-distance communications, require antennas to have low sidelobe and high gain characteristics. One simple and convenient solution is to employ several, often identical, antennas into an array. Together, the radiating elements can be configured to achieve directional radiation patterns and high gain. A linear array of four elements, capable of forming a directive beam, will also be to that end.

This chapter is focused on the design of the design of the slot array and the connecting CPW between them. The array is composed of four slot elements arranged as two pairs of bidirectional, series-fed segments (Figure 4.1). Prior to designing the array in simulations, a precursory analysis of array theory was performed to predict the far field behavior of the four elements. Simulated and measured results of return loss and radiation pattern for the functional array will be presented here.

The planar (linear) array employed in this design is composed of four slot elements which provide a directive and steerable major beam.

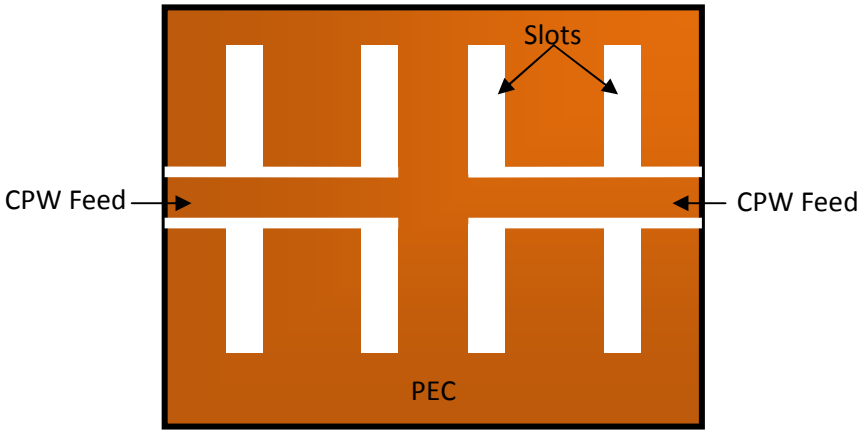

Figure 4.1 - Basic Layout of Four-Element Linear Array.

4.2 Array Analysis

The initial aim of this work was to produce a uni-directional antenna from a bi-directional planar, slot array. Each planar segment consists of a four-element slot array. Two feeds, arranged bi-directionally, will excite the each of the series-fed segments (Figure 30). The array was designed to produce a directive major lobe at broadside which is both narrow in phi but broad in theta. When an offset phased is introduced into one of the segments, the beam can be tilted off broadside.

The radiation pattern of linear arrays can be described by and controlled by the relative spacing of the elements in the array, the amplitude and phase of each element or some combination of the three. However, there is a direct trade-off between the

directivity of the major lobe, and the amount of power lost in side-lobe radiation. As the major beam at broadside is gradually "squeezed" by adjusting element spacing, the array will beget sidelobes. The design will intend to keep gain high and sidelobe levels low.

Prior to examining the slot layout in simulation, a parametric analysis was done to investigate the effects of element spacing, amplitude and feed-phase of the four-element, linear array. This mathematical approach is an ideal interpretation of the destructive and constructive effects of four, infinitesimal point-sources radiating in freespace. The analysis neglects some actual contributing factors including: equal power distribution, current distribution and coupling, but is meant to be a precursory exercise to demonstrate how the individual elements in the array will govern the total radiated pattern.

Mathsoft's MathCAD was used to plot the radiation intensity of the four infinitesimal dipoles arranged in a linear array. Using simple array theory (Equations 14 and 15), the pattern produced by the linear array can be calculated from the array factor, and, in turn, by the radiation intensity. The radiation of each element can be fully described by its amplitude (a_1, a_2), feed phase (Φ_1, Φ_2) and physical, freespace separation (d_c , d_o) from the geometric center of the array.

$$AF(\theta) = a_1 \cdot e^{-j\cdot k\cdot d_o\cdot \cos(\theta)} \cdot e^{j\cdot \Phi_1} + a_2 \cdot e^{-j\cdot k\cdot d_c\cdot \cos(\theta)} \cdot e^{-j\cdot \Phi'_1} + \quad (14)$$

$$a_2 \cdot e^{-j\cdot k\cdot d_c\cdot \cos(\theta)} \cdot e^{-j\cdot \Phi'_1} + a_1 \cdot e^{-j\cdot k\cdot d_o\cdot \cos(\theta)} \cdot e^{j\cdot \Phi_1}$$

$$U(\theta) = \frac{(|AF(\theta)|)^2}{(|AF(90°)|)^2} \tag{15}$$

Figure 4.2 shows the four point sources arranged in a linear array and radiating with equal amounts of power. The normalized radiation patterns of the array, plotted with Equations 14 and 15, are shown with incremental, uniform spacing of *d* between all of the elements; distances are given in terms of the freespace wavelength of the 5GHz center frequency.

The patterns show that closely-spaced elements produce broad, bi-directional major lobes at broadside (90° and 270°). Increasing the spacing between the elements makes the major lobe more directive (Figure 4.3). However, this does not come without consequence. As energy is increasingly focused at broadside, radiation will also grow in the sidelobes.

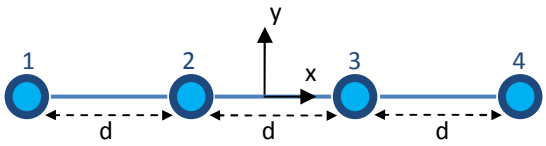

Figure 4.2 – Four-element Array of Point Sources with Uniform Spacing.

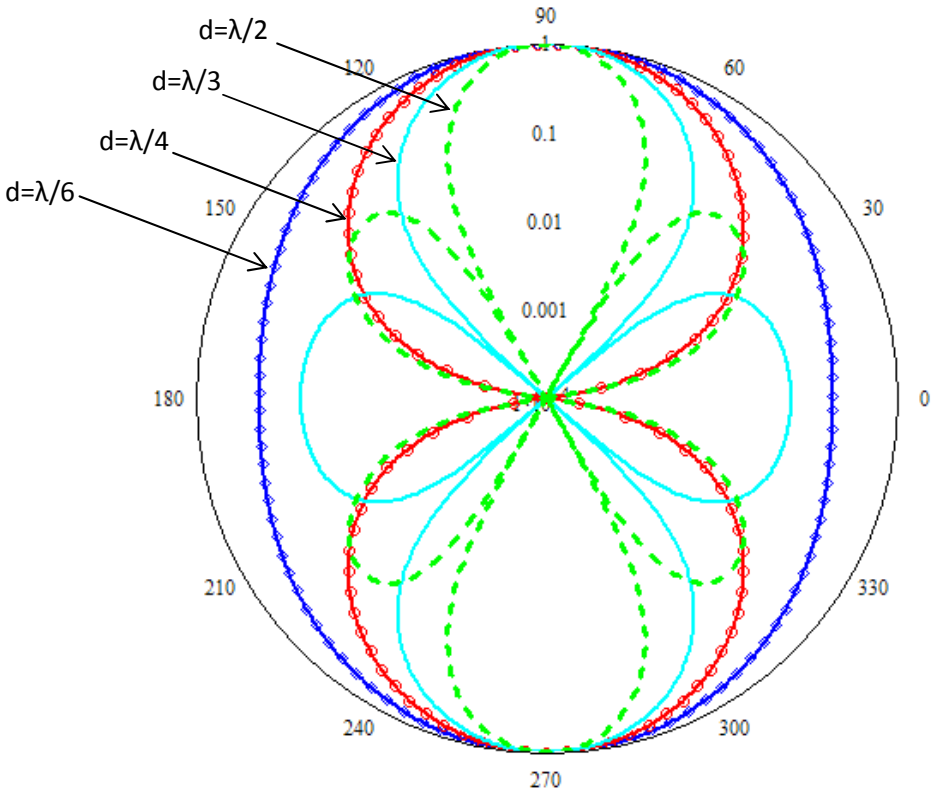

Figure 4.3 - Radiation Intensity of Elements Spaced Uniformly.

In this work, the two inner elements are linked to their respective, neigboring, outer elements by a series feed. This CPW feed between them will restrict their relative movement in freespace. To account for this limitation, the outer element spacing *d* of

Figure 33 was fixed at $\lambda_0/2$(freespace wavelengths), while the inner spacing d_1 between the pairs was altered to see its effects on the radiation pattern. As was similarly shown in the uniformly spaced array, increasing the distance d_1 between the two pairs will directly control the directivity of the major lobe and size of the sidelobes. A center spacing of $d_1=\lambda_0/4$ has a relatively directive major beam and no detectable, extraneous lobes. Extending the spacing further causes the major lobe to narrow at broadside but sidelobes grow considerably.

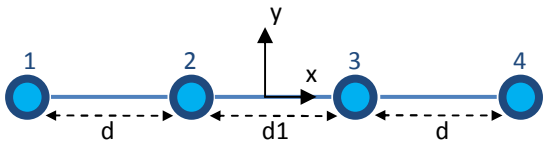

Figure 4.4 – Four-element Array of Point Sources with Fixed Outer Spacing and Varied Inner Spacing.

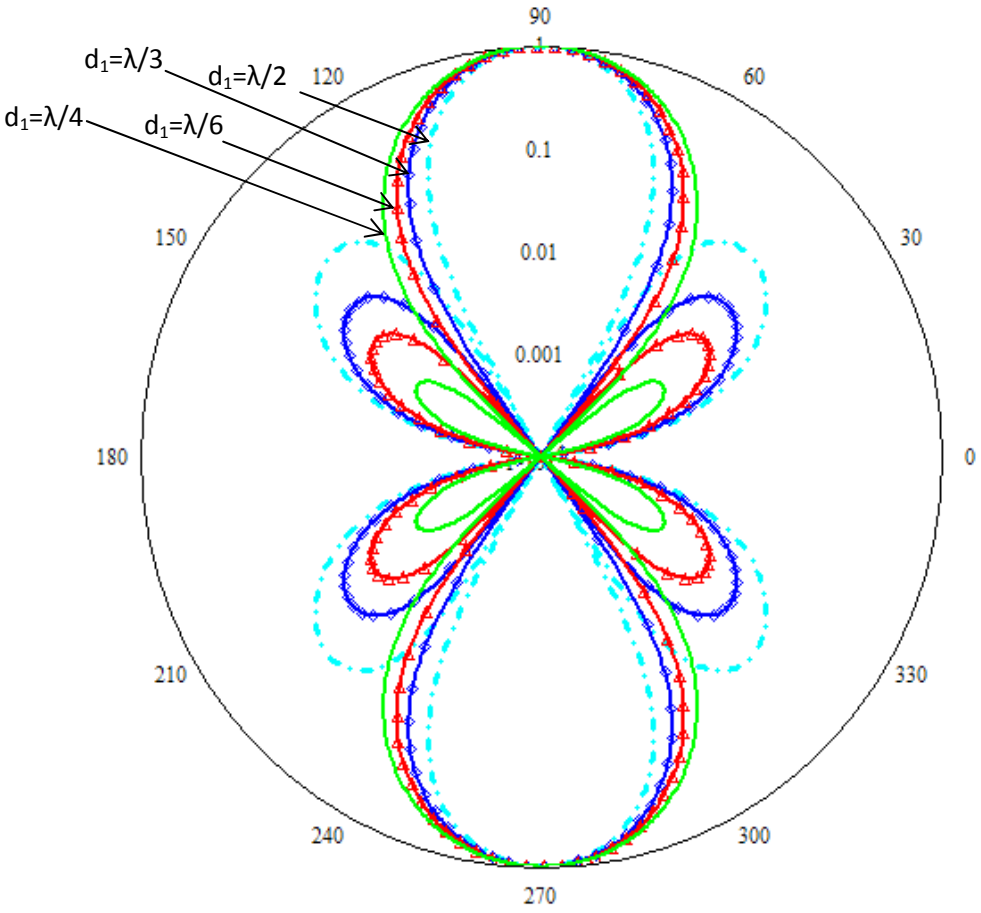

Figure 4.5 – Normalized Radiation Intensity of Four-element Array with Altered Center Spacing.

The array analysis shows that the directivity of the major lobe at broadside can be drastically increased by spacing the elements far apart, but is eventually restricted by the growth of grating lobes. A uniform spacing of $d=\lambda/4$ yields two major lobes (front and back) with no detectable sidelobes. As spacing is increased, the major lobes become narrower, but the sidelobes grow significantly.

4.3 Mutual Impedance

The array analysis is useful in understanding how the four-element array will shape the far-field pattern, but having the elements in close proximity will inevitably give rise to mutual affects. In addition to the coupling from the radiated fields, all of the slots will also share the ground plane. This will alter the current distribution and, thus, input impedance. Mutual impedance plays an important role in antenna performance because it is the driving port impedance that must be matched. The mutual impedance of two side-by-side dipoles is given as

$$Z_{1(\text{input})} = \frac{V_1}{I_1} = Z_{11} + Z_{12}\left(\frac{I_2}{I_1}\right) \tag{18}$$

$$Z_{2(\text{input})} = \frac{V_2}{I_2} = Z_{22} + Z_{21}\left(\frac{I_1}{I_2}\right) \tag{19}$$

Each element creates its own self-impedance (Z_{11} and Z_{22}), but also experiences some additional impedance from the neighboring element(s) (Z_{12} and Z_{21}). Mutual impedance is quite complex to analyze mathematically, so MOM was used to directly measure the effects of two slots as a function of their freespace separation.

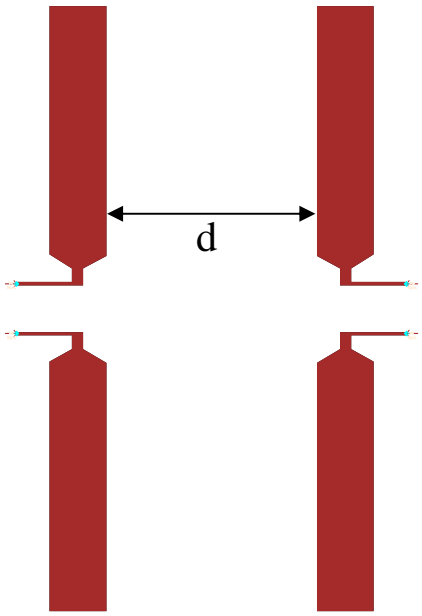

Figure 4.6 – Layout of Mutual Impedance Measurements

Two slots were arranged as shown in Figure 4.6. Each slot had already been previously matched to a 50Ω port. The mutual impedance, then, is the variation (from 50Ω) in either of the slot's input impedance after they have been simulated together. The simulated, mutual affects are plotted in Figure 4.7. As would be expected, coupling is stronger for smaller spacing between the two slots and decays as the spacing increases. The highest, simulated, mutual impedance was -17Ω at $d=0.08\cdot\lambda_0$.

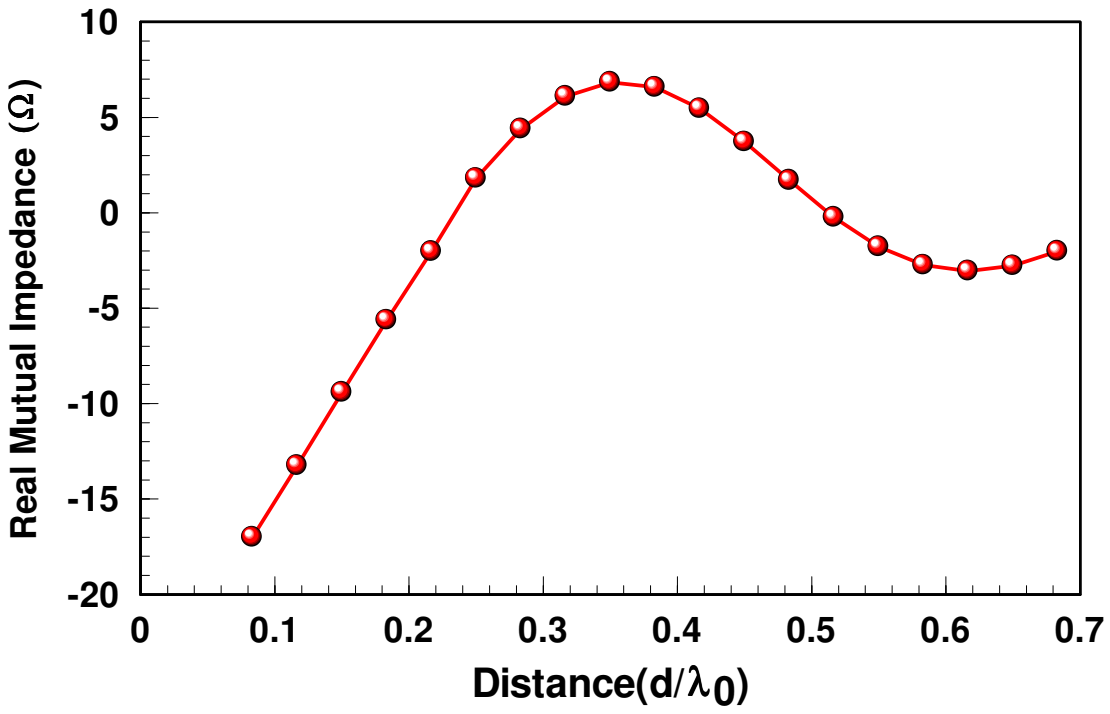

Figure 4.7 – Simulated Mutual Impedance

4.4 Feed Effects

The array theory uses ideal elements to examine the radiated far field, but to practically feed all four elements, some feedline must be placed between them. The dimensions of the feed, up to now, were somewhat insignificant. In the design of the single slot given in Chapter 3, the feed effects could be negated by shifting the reference plane to the base of the slot. These effects, though, are real and must be factored into any prudent array design. Expanding the single slot into the two-element series-fed array of two slots, the CPW feed must be extended some distance away, where the second can be affixed. The characteristic impedance, and therefore feed dimensions, of the line was determined first; the slot was subsequently built around it. The feed is pivotal to the proper functioning of the array and its effects are addressed here. Once element spacing is decided, the mutual impedance can be corrected by tuning the slots back to 50Ω.

4.4.1 Guided Wavelength

The electric field lines of the traveling, slow-wave are evenly split between the air above and substrate below as it is transmitted through the CPW line. In theory, a substrate of infinite thickness has half of the EM field lines contained within the substrate below and the other half within the air above. Thus, the effective permittivity (ε_{eff}) is taken to be the average of the two:

$$\varepsilon_{eff} = \frac{\varepsilon_{r1} + \varepsilon_{r2}}{2} = \frac{1 + \varepsilon_{r2}}{2} \tag{20}$$

The guided wavelength (λ_g), then, is the scaled freespace wavelength and is given as

$$\lambda_g = \frac{c}{f \cdot \sqrt{\varepsilon_{eff}}} \tag{21}$$

where *c* is the speed of light and *f* is the frequency of interest. A substrate of infinite thickness is implausible, but the same assumptions will apply for relatively thick substrates where most of the lower field lines are still contained within the substrate (Figure 4.8).

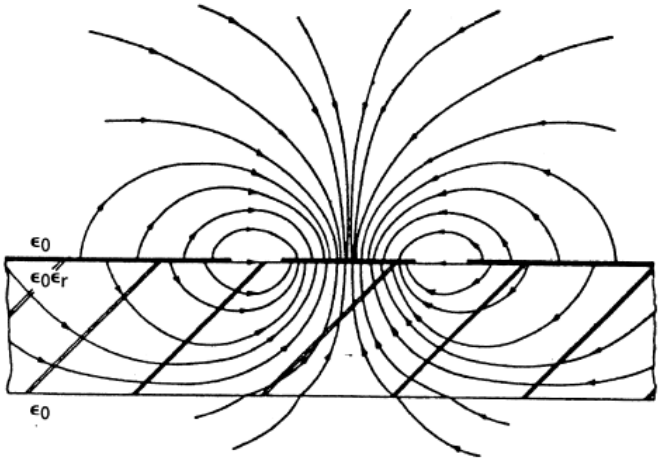

Figure 4.8 - Electric Field Lines for a Conventional CPW of Finite Dielectric Thickness

4.4.2 CPW Characteristic Impedance

The conventional CPW structure is on a single dielectric substrate and without a ground plane on the backside of the dielectric. Its few variable dimensions can be adjusted to set the desired, characteristic impedance of the line. These features are: the signal(S), gap widths (w), substrate height (h) and substrate permittivity (ε_r) of the CPW, and are sufficient to fully describe its characteristic impedance (Figure 4.7). The proximity of the signal line to the ground plane will dominate the capacitance of the line and, in turn, the line's characteristic impedance.

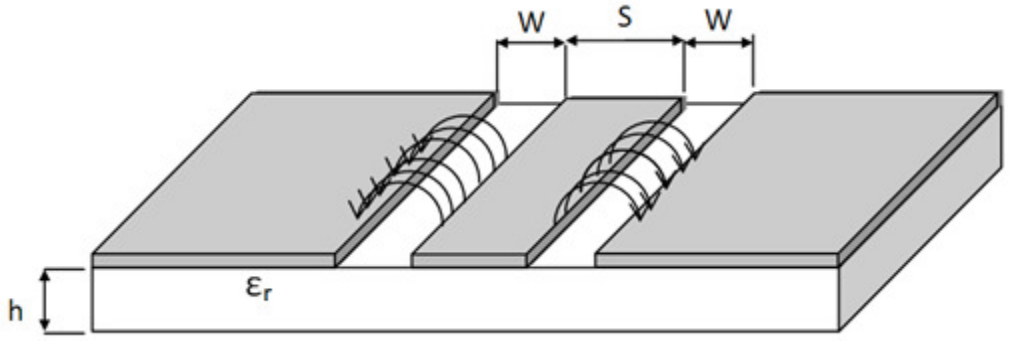

Figure 4.9 – Structure of CPW Feedline

While all line impedances are theoretically possible, extremely high and low characteristic impedances are difficult to achieve as they require that the signal width(*s*) to become very large or gap width (*w*) to become very small. Some consideration must also be given to feasible fabrication dimensions including: minimum milling features, connector sizes, and overall footprint. For the relative dimensions and scale of this design, characteristic line impedances between 30Ω and 75Ω were practical.

Table 4.1 - Signal Width and Slot Dimensions for Given Characteristic Impedance.

Characteristic Impedance=25Ω		Characteristic Impedance=50Ω		Characteristic Impedance=100Ω	
W-Width(mm)	S-Signal(mm)	W-Width(mm)	S-Signal(mm)	W-Width(mm)	S-Signal(mm)
0.10	168.745	0.10	1.133	0.10	0.082
0.25	168.809	0.25	3.530	0.25	0.220
0.50	168.805	0.50	9.719	0.50	0.463

Table 4.1 shows how the characteristic impedance of a line will drastically alter its dimensions. For a line of 25Ω characteristic impedance, a signal width of 168mm is required, nearly 400% larger than the slots themselves. At the other end of the scale, a line of 100Ω characteristic impedance has a very narrow signal width and large gap width.

4.5 Series Feed

4.5.1 Impedance Transformation

The design was aimed to evenly match the series-fed slot elements to radiate power evenly. For this to happen, the CPW feed between the two slots should not alter the input impedance of the second slot.

$$Z_{in}(d) = Z_0 \frac{Z_L + i \cdot Z_0 \cdot \tan(\beta d)}{Z_0 + i \cdot Z_L \cdot \tan(\beta d)} \quad (22)$$

The addition of this feed-line transforms the input impedance of the single slot as given by Equation 22 which says that the impedance looking into the feed line (*Zin*) at some distance of feed away (*d*) is described by: the input impedance of the single slot (Z_L), the characteristic impedance of the transmission line (Z_0) and the propagation constant (β, given in degrees/mm). Unless the feed is used for impedance matching, its characteristic impedance should be equal to the input impedance of the slot itself. Figure 4.6 demonstrates how impedance matching can be accomplished with the feedline.

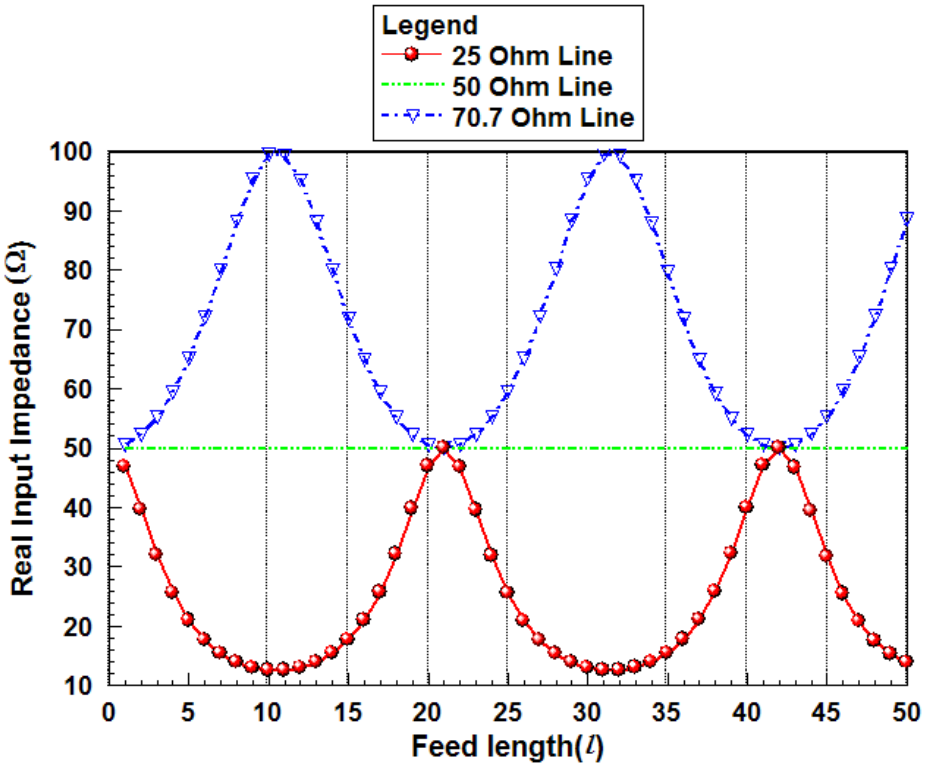

Figure 4.10 – Impedance Transformation with Feedline.

In accordance with Equation 22, feeds of three different line impedances (with assumed identical propagation constants) are used to feed a 50Ω load. At the load (*l=0*), all three lines produce equal input impedance, identical to the load. Moving away from the load along the line, their effects become pronounced. The 50Ω line is matched to the load and will never alter the impedance, only phase. The 70.7Ω and 25Ω lines have a variable effect on the impedance which is a function of the feed length. At odd multiples of a quarter guided-wavelength ($n \cdot \lambda_g/4$, *n=1, 3, 5...*) the impedance transformation is the most significant where

(23)

$$Z_{in} = \frac{Z_0^{\,2}}{Z_L}$$

The lines have no effect at even multiples of a quarter wavelength ($n \cdot \lambda_g/4$, *n=0,2, 4...)*; the input impedance is identical to the load impedance. Between these two extremes, any input impedance can be achieved by choosing the corresponding feed length.

4.5.2 Feed Phase

The characteristic impedance of the CPW line will be chosen to match the impedance of the slot (50Ω). Therefore, the impedance will not (ideally) be shifted at any distance away from the radiating element. The length, however, will shift the phase of the transmitted signal. To ensure that the slots are being fed in-phase, the electrical length between any two similar points on the slots should be some multiple of a guided wavelength ($n \cdot \lambda_g$, *where n=1,2,3..*). That is to say, the electric path around the slot will account for some change in phase of the signal. Usually the path around the slot accounts for exactly a whole wavelength, and, therefore, the feed itself will also be one full cycle in length. The CPW feed, then, will be set so that the voltage will rise and fall across along the slots' edges in concert. That way, their combined radiation effects are the constructive formation of a single, bi-directional beam at broadside.

The length of this feed will set the freespace separation of the slots and may not align with the preferred freespace separation as determined in the array analysis. Also, the series-fed is a limitation in the spatial economy of the overall array. To reduce the overall footprint of the array and/or allow flexibility of spacing between the series-fed elements to improve gain or reduce sidelobes, the feed can be meandered.

The phase of the feed can be verified by removing the slot from the end of the CPW line and replacing it with a port. The phase of the transmitted signal, S_{21}, will exhibit a zero-crossing for each full rotation.

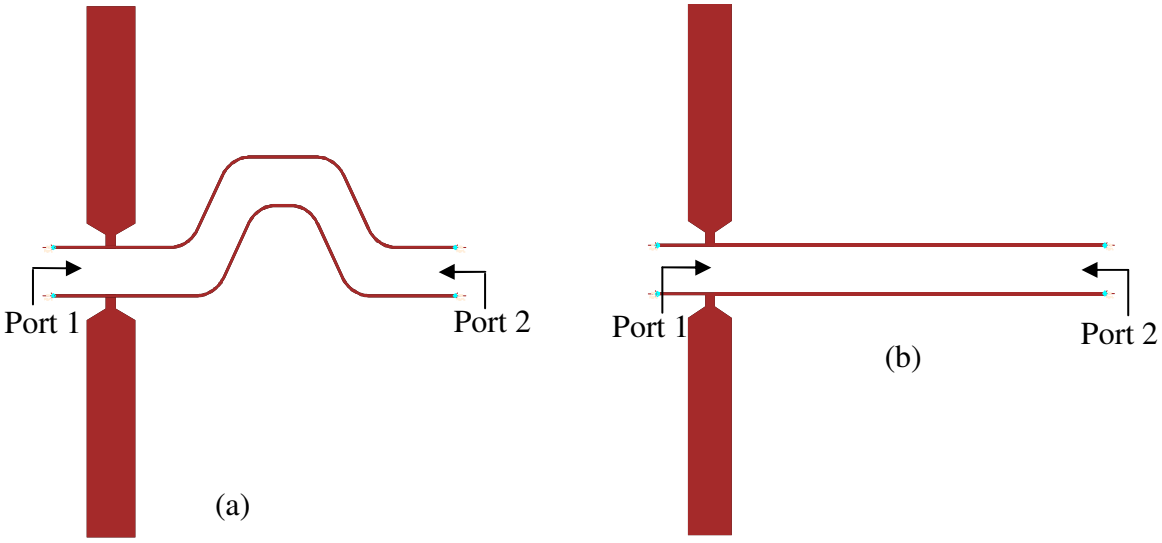

Figure 4.11 – Straight (a) and Meandered (b) CPW Feed.

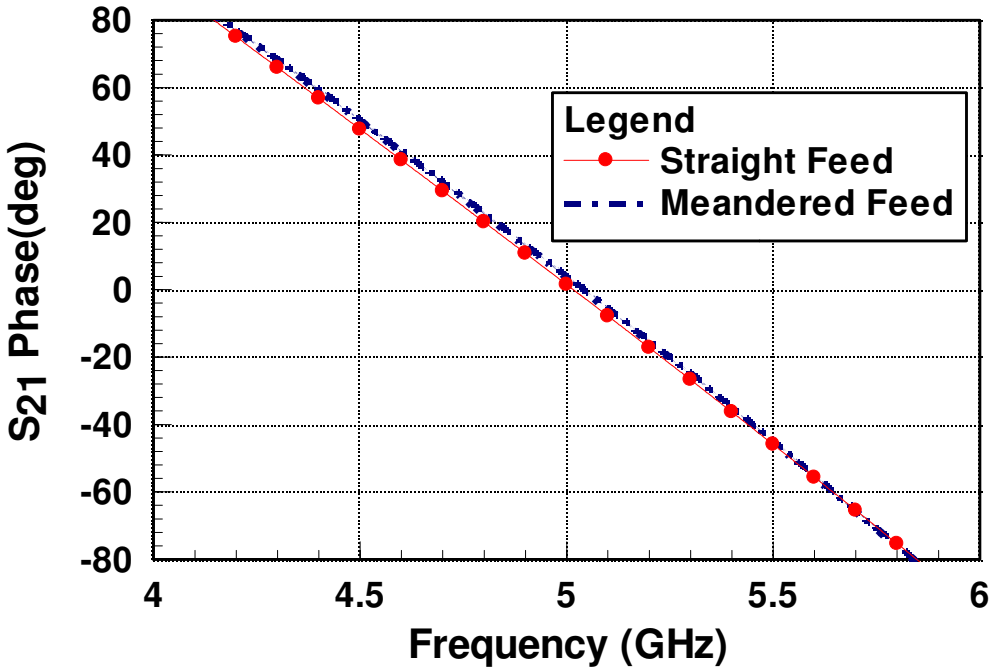

Figure 4.12 – Phase of S_{21} for Straight and Meandered Feed.

The 0° phase crossings of S_{21} in Figure 4.8 are an indication that the signal fed into port 1 is in phase with that received at port 2. Both the straight and meandered CPW feeds are of equal length and exhibit this behavior, thus verifying that the meandered feed will not alter the phase of the signal and can be used to properly feed the array. When port 2 is replaced with a second slot, the elements will be operating in phase.

4.6 Planar Array

To construct the series-fed segments, two slots are placed half of a freespace wavelength apart ($d=\lambda_0/2$) and with a 50Ω CPW feed at their center; the feed dimensions are determined by ADS' Linecalc. The slot lengths and widths are adjusted until a strong resonance around 5GHz is achieved by matching the slots to the feed and nullifying the effects mutual impedance. A meandered 50Ω line of a one guided wavelength (λ_g) is

then used to adjoin the two slots. The summation of the two 50Ω slots yields a 100Ω impedance at the input. Employing impedance matching with the feed that is before the array, a 70.7 Ω quarter-wavelength line is used to convert the 100Ω impedance back to the desired, nominal 50Ω (Figure 4.9). The signal width was kept fixed at 4mm while gap width was increased to achieve the higher characteristic impedance.

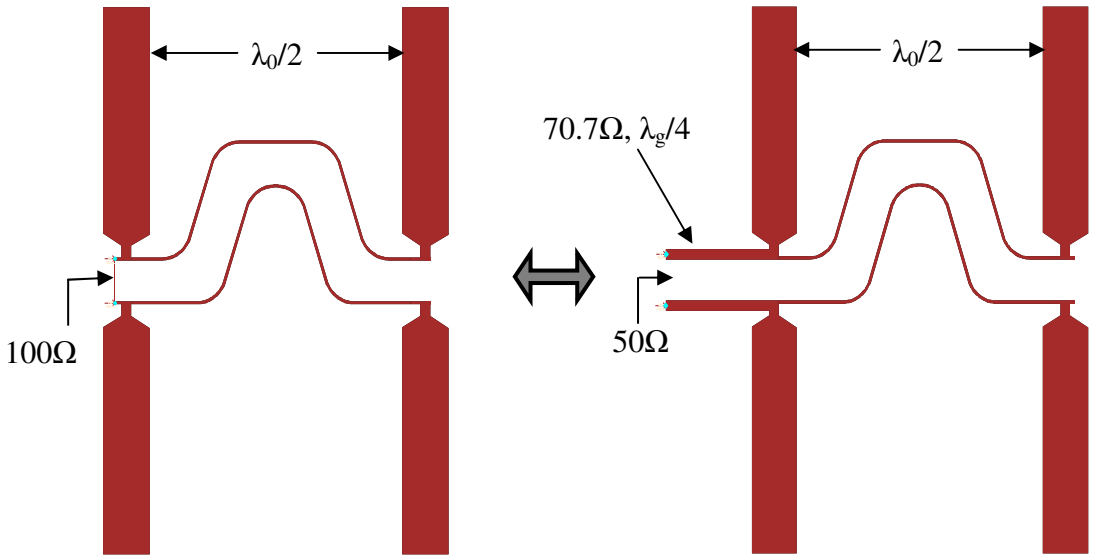

Figure 4.13 – Quarter-wave Matching, 100 Ω to 50 Ω.

The two-element array is now matched for a 50Ω input; mirroring it about itself will give the full planar array; the two inner slots were kept at half a freespace wavelength ($\lambda_0/2$). The 70.7Ω impedance line was again reduced back to the 50Ω impedance and extended away for the connectors to be mounted. To compensate for the direction of the feed, an additional 50Ω line of 180° was added to one of the segments (Figure 4.13). This phase offset would otherwise be provided by a phase shifter, peripheral to this work.

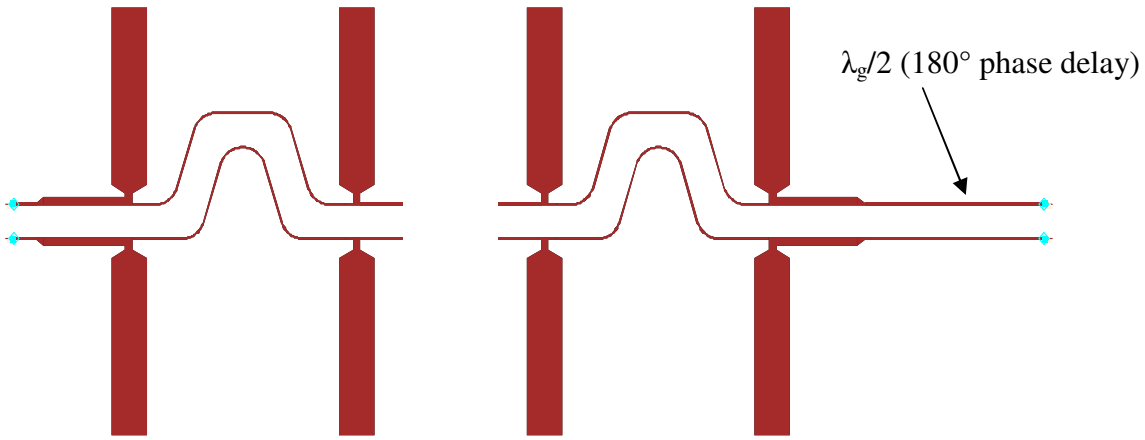

Figure 4.14 – Full Array with Feed Offset .

To verify that the slots are operating in-phase, the current distribution is again plotted in Figure 4.14. The plot shows that all four slots are simultaneously experiencing strong current distribution along their edges, indicative of in-phase resonance for the wavelength-long elements.

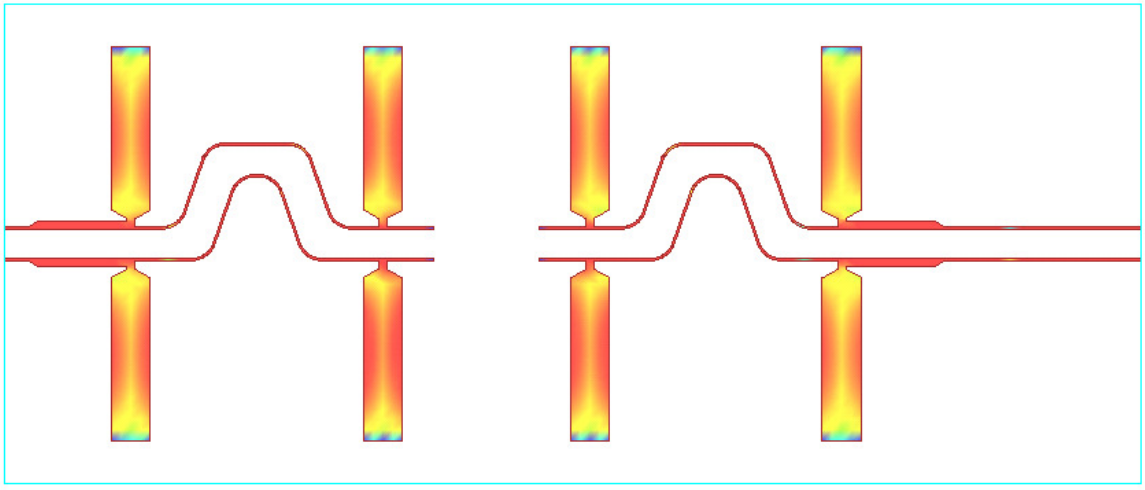

Figure 4.15 – Current Distribution of Full Array.

If the elements are not radiating in-phase, cancellation and unwanted nulls could occur in the radiated far field. The symmetry of the design helps to abate any minor length or impedance differences that may arise.

The array is fed bi-directionally at each of its end by two separate ports. Nominally, the ports will be 180° out of phase (to account for the direction of the feed) and the major beam will be fixed at broadside. A phase shifter, external to this design, can provide continuous phase control of one of the feeds. As the phase between the elements is progressively changed, the major lobe can be swept off broadside. The amount of possible tilt is, again, limited by the rapid growth of sidelobes.

4.7 Results and Comparison

Figure 4.15 shows the fabricated planar array with soldered connectors. The board was milled into a 60mil, Rogers 4003C (ε_r=3.55) board. Measured and simulated RL plots (Figures 4.17 and 4.18) roughly align, but the apparent shift is likely caused by an imperfect impedance match between the CPW line and the coax-to-CPW connector.

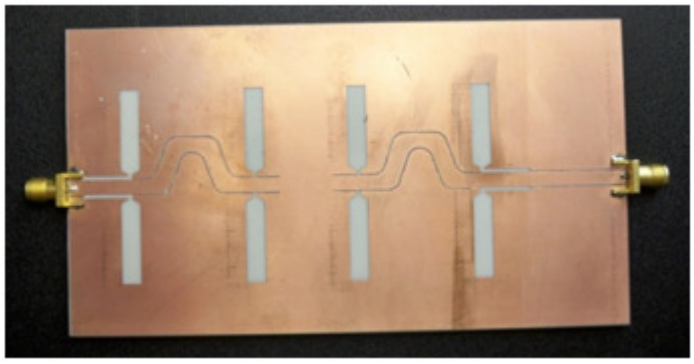

Figure 4.16 – Fabricated Printed-slot Array.

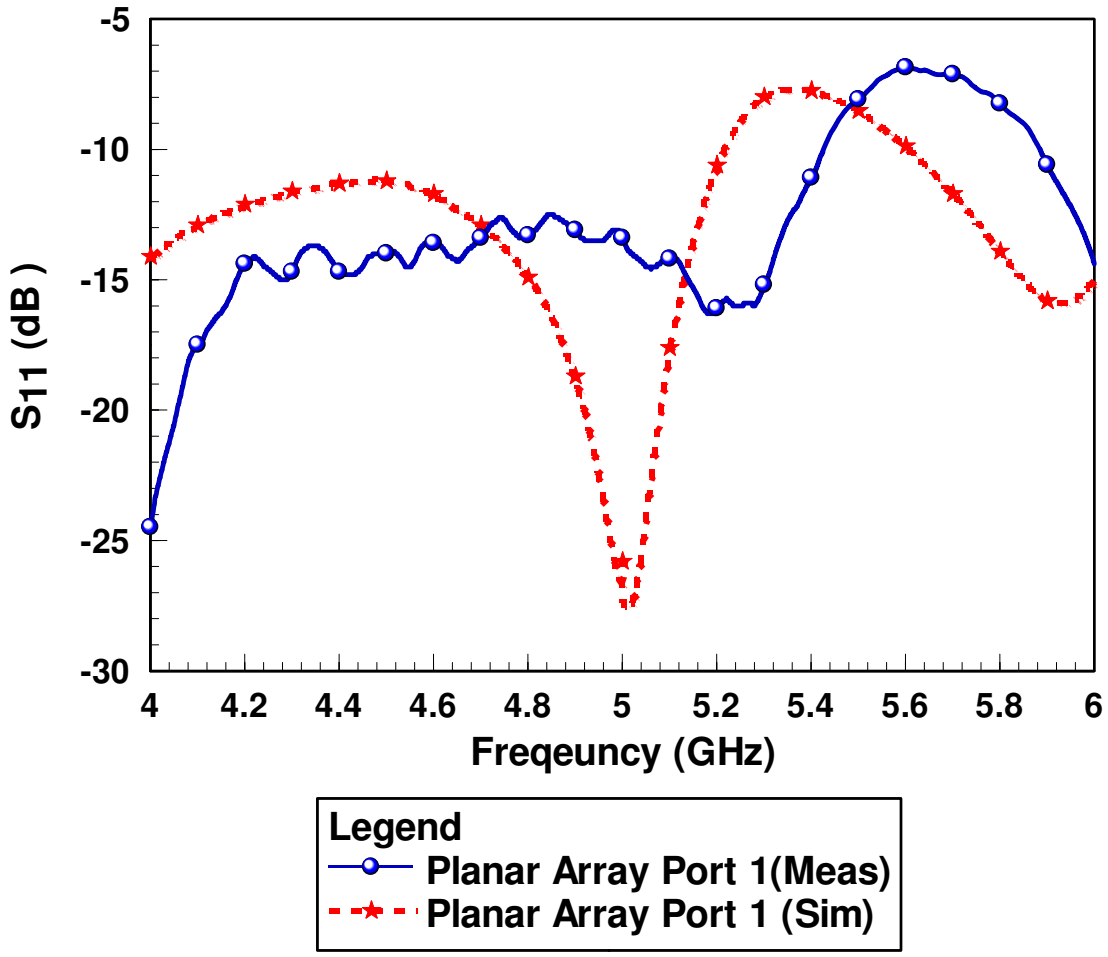

Figure 4.17 – Return Loss for Port 1 of Planar Array.

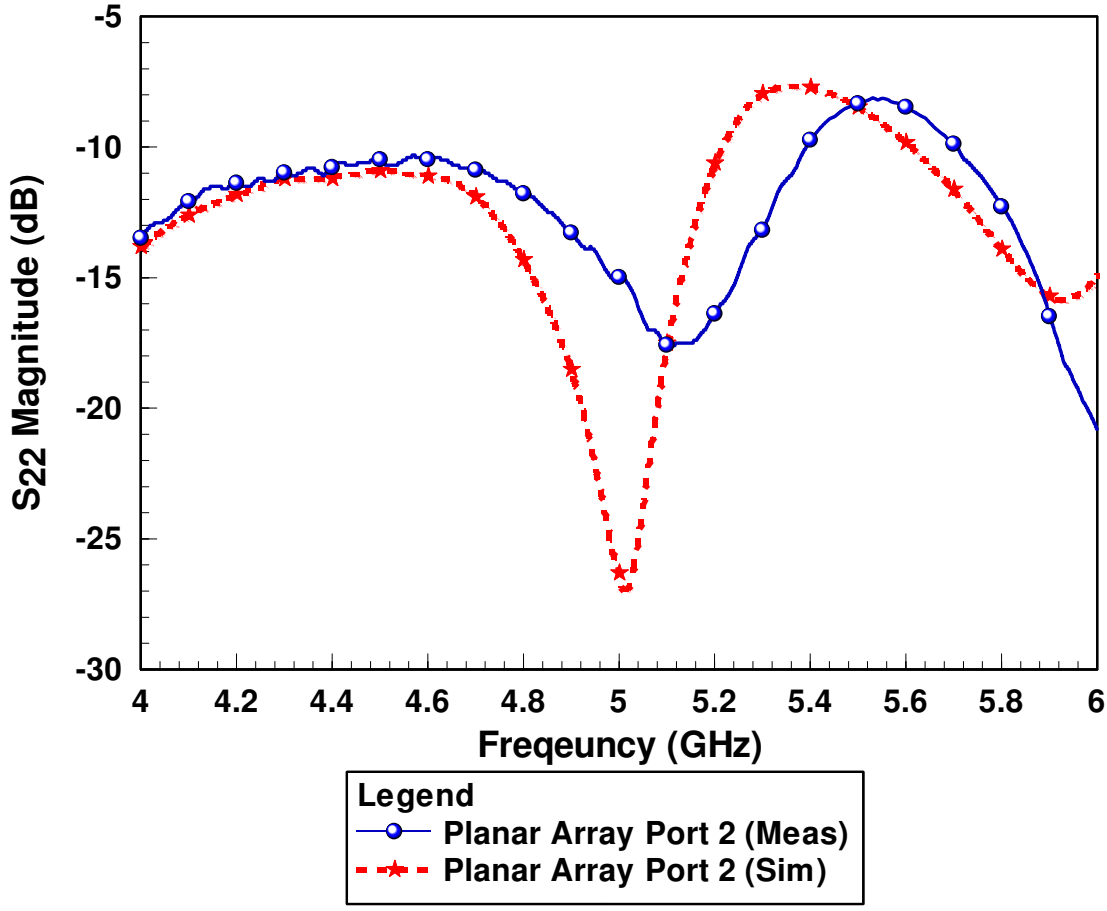

Figure 4.18 – Return Loss for Port 2 of Planar Array.

Both plots demonstrate a bandwidth greater than 28%. The return loss stays well above the 10dB mark below 4GHz lower limit that has been examined throughout the design process, but the additional bandwidth is of little consequence to this work.

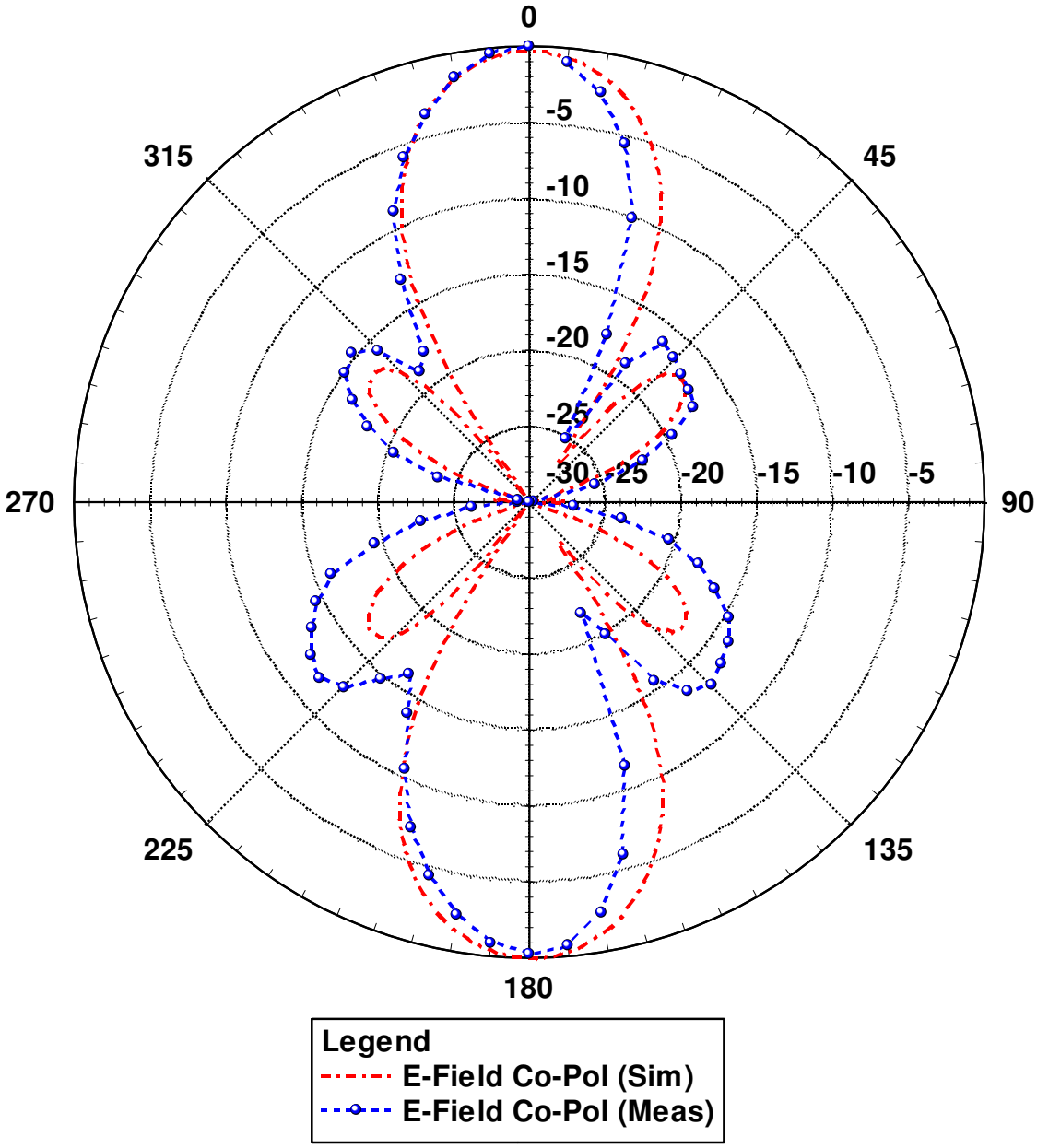

Figure 4.19 – Simulated vs. Measured E-Co Pattern.

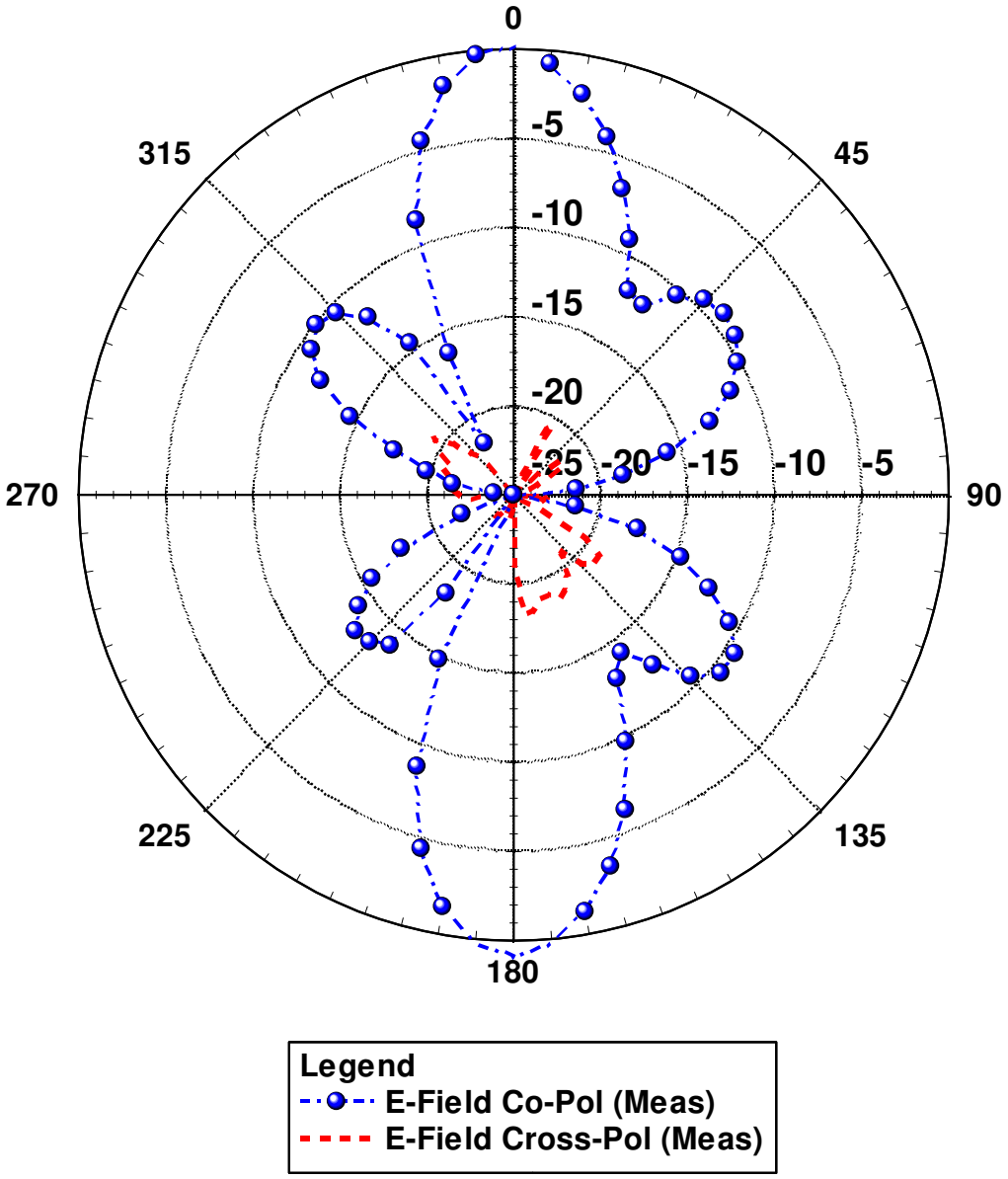

Figure 4.20 –Measured E-Co vs. Measured E-Cross.

The E-field co-polarization cut of Figure 4.19 demonstrates a directive major lobe at broadside for both simulated and measured patterns. The measured sidelobe levels were ~12dB down from the major beam and about 5 dB higher than simulated. It should be noted that the measured array also produced a narrower major beam which would,

understandably, result in higher sidelobe levels, as predicted by the array model. The measured E-field cross-polarization (Figure 4.20) is, at its peak, much lower (~18dB down) than the maximum co-polarization in the E-plane.

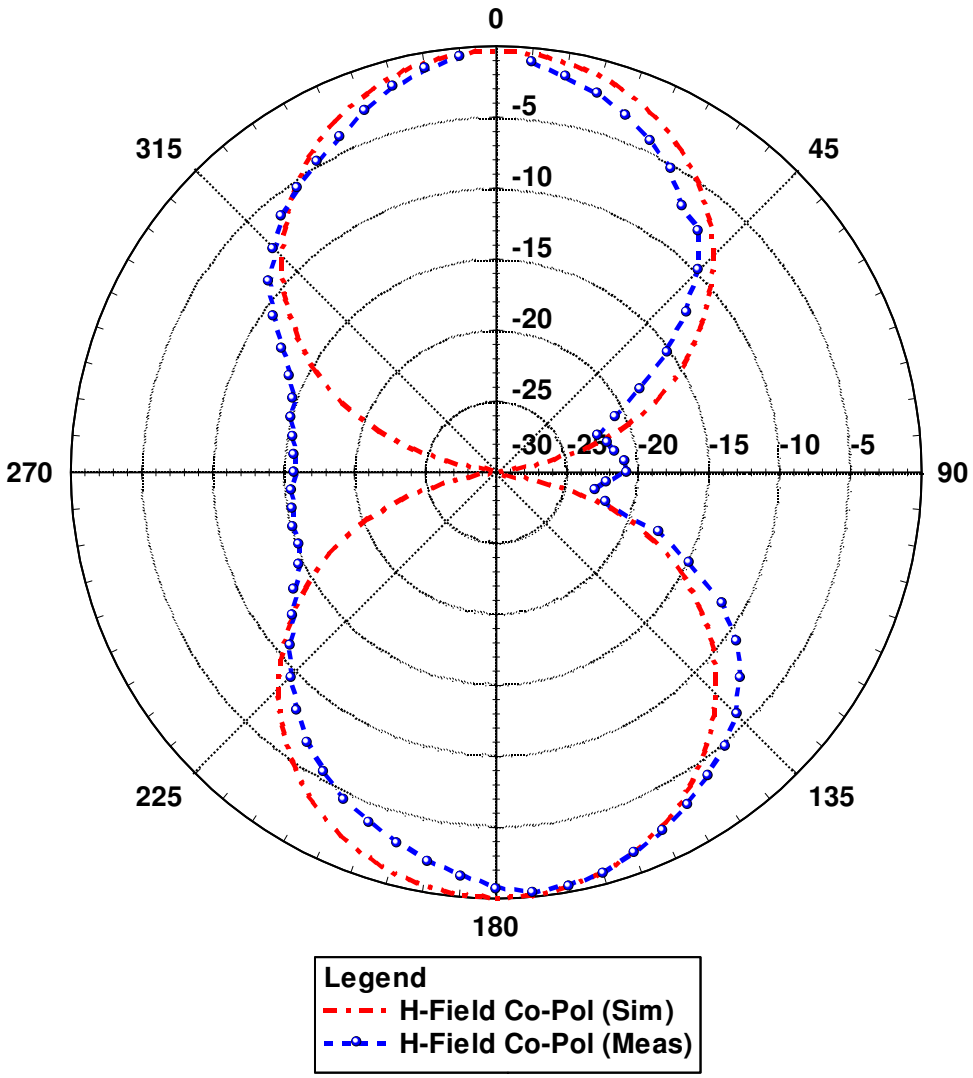

Figure 4.21 – Simulated vs. Measured H-Co Pattern.

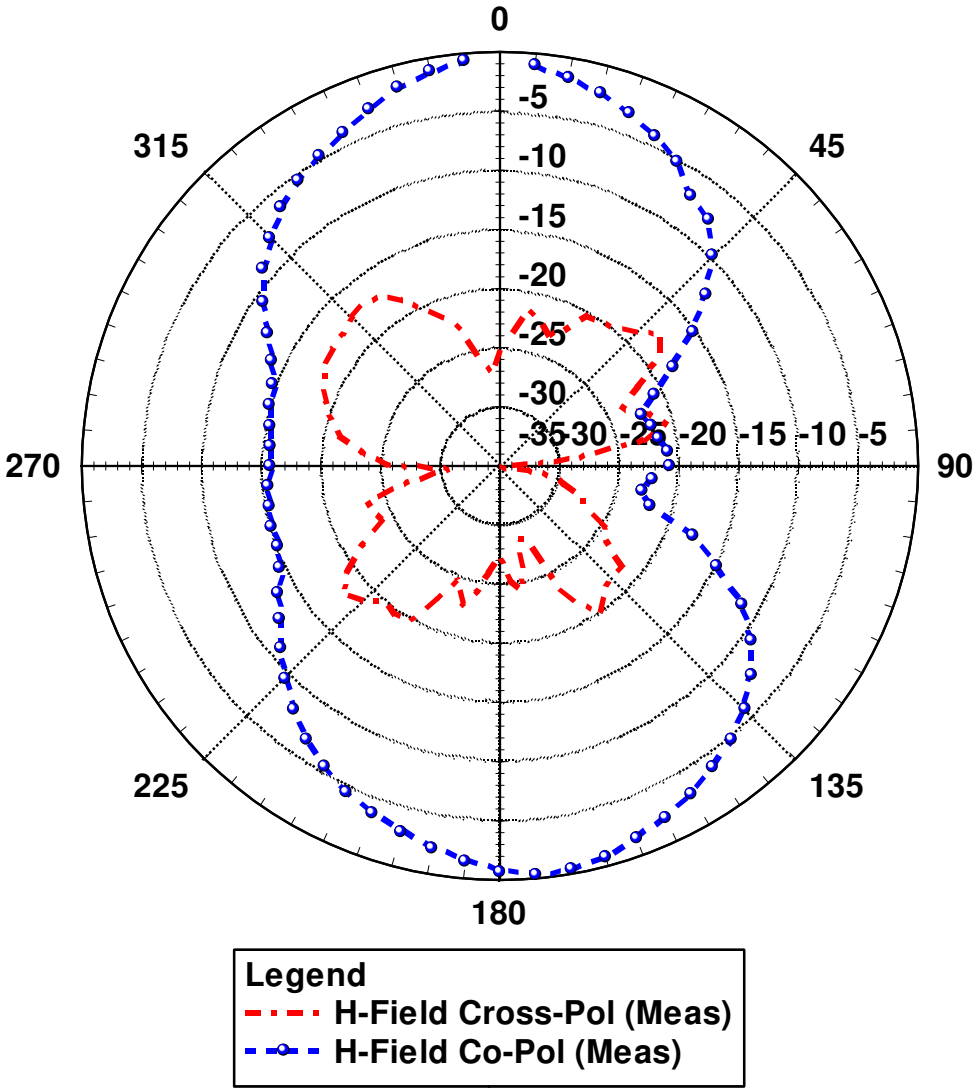

Figure 4.22 - Measured H-Co vs. Measured H-Cross.

The measured H-field radiation patterns are shown in Figures 4.21 and 4.22. Plots of measured and simulated co-pol patterns are nearly identical in shape and beamwidth. Cross polarization levels in the H-plane also stay more than 17dB down from the peak co-polarization levels. Deep nulls are apparent in the plane of the array for the simulated patterns because the infinitely long metal sheets assumed in Momentum prevent the radiation of parallel waves.

4.8 Chapter Summary and Conclusions

A four-element slot array was designed based on the rectangular slot of Chapter 3. A mathematical array analysis helped determine how array spacing would shape the far-field radiation pattern. Momentum was used to show that there is a strong relationship between slot spacing and mutual impedance that must be considered in the array design. The signal and gap widths of the series, CPW feed were designed to avoid any impedance transformation at center frequency and its length was set so that the slots were radiating in-phase. The slots were individually tuned for 50Ω input impedance around the CPW feed, combined in-series and then reduced back to 50Ω with a quarter-wave matching line. The measured return loss varied slightly from the simulated return loss, most likely this can be attributed to the connector. Measured and simulated pattern measurements also showed close alignment, with measured cross-polarization significantly lower than co-polarization measurements in both E and H planes.

CHAPTER 5

CAVITY-BACKED PLANAR ARRAY

The CPW-fed slot inherently radiates bidirectional and, for this reason, has had little use as a conventional, uni-directional radiator. There are several approaches to restrict radiation to above the groundplane and recover that power so that it may be constructively added to the fields in the opposing half-space. Lenses, grounded substrates and metallic reflectors were considered.

5.2 Methods for Restoring Backside Radiation

5.2.1 Slots on Lens

Dielectric lenses in direct contact with the radiating ground plane are one method to attain uni-directional radiation. A high-dielectric lens can be placed as a superstrate atop the ground plane. The original, thin substrate and air on the backside of the ground plane will have much lower effective permittivity than thick dielectric lens on the opposite side. The superstrate, therefore, will contain most of the field, causing most of the power to be radiated through the lens and greatly reduce radiation in the backside. The shape of the lens will tend to focus the field.

Lenses can be used to impedance match between interfaces and their construction is typically extremely durable. They do, however, have many drawbacks. Fields that

travel through thicker portions of the lens may suffer from considerable more power loss if the lens is dissipative [28]. Sometimes lenses are made from many dielectric layers, making them difficult and expensive to produce. The efficiency of lenses is low because unwanted reflections occur on both the front and rear surfaces. Also, they are usually multiples wavelengths thick and only reasonable for higher frequencies where the wavelength is small.

5.2.2 Grounded Substrates

The CPW-fed rectangular slot and loop antennas (Figure 5.1) have grounded substrates, making them inherently unidirectional. These structures often require many dielectric layers of varying permittivity to prevent parallel plate TEM modes between the two metal sheets [25]. Both the slot and loop designs had low radiation efficiencies, 36% and 54%, respectively.

Figure 5.1 - Slot Antenna (a) and Loop Antenna (b).

5.2.3 Reflectors and Cavities

Probably the simplest and cost-effective method for achieving uni-directinal radiation is a metallic reflector placed behind the array. When positioned a quarter-wavelength away from the array, the flat reflector will reflect most backside radiation. The quarter-wave spacing of the reflector is pivotal in its functioning and will ensure that the reflected power will be wholly added to that power radiated in the front side.

In addition to the quarter-wave, finite, metal plate, the cavity has walls which will fully enclose the backside of the array and help prevent backside radiation leakage. In theory, a properly designed cavity could double the gain of the antenna. The cavity can also be loaded with a dielectric to further shrink the size (depth) of the total assembly, but will come at the expense of reduced bandwidth and efficiency. An air-filled cavity will be pursued here as it is the simplest.

5.3 Design of Cavity-backed Array

Most of the design, up this point was carried out in Agilent's ADS. However, because of the increased complexity that this cavity-backing introduces, Ansoft's HFSS was used for the full and final design. The addition of the cavity does not leave the array performance unaffected and the change in CAD tools required that some design features be changed.

The close proximity of the metallic cavity structure causes parallel-plate capacitance between itself and the ground plane of the array. The increased capacitance will decrease the characteristic impedance of the slot dimensions. Through certain design

modifications, the cavity effects can be corrected. The meandered feed was mitered at its bends to mitigate parasitics. The freespace separation used in the planar array was preserved here so that any improvements in gain could be considered a product of the cavity addition. An approach similar to that used for the planar array was used for the cavity-backed array. First, a single slot was tuned to be matched to the driving port and function within the cavity. These dimensions were verified to have strong resonance centered at f_c and transferred to the full array. Freespace separation was set for the four elements and the meandered feed was altered until the elements were radiating in phase. All dimensions were tuned until matched to the driving port. The layout of the final array is shown in Figure 5.3 with the relevant dimensions in Table 5.1.

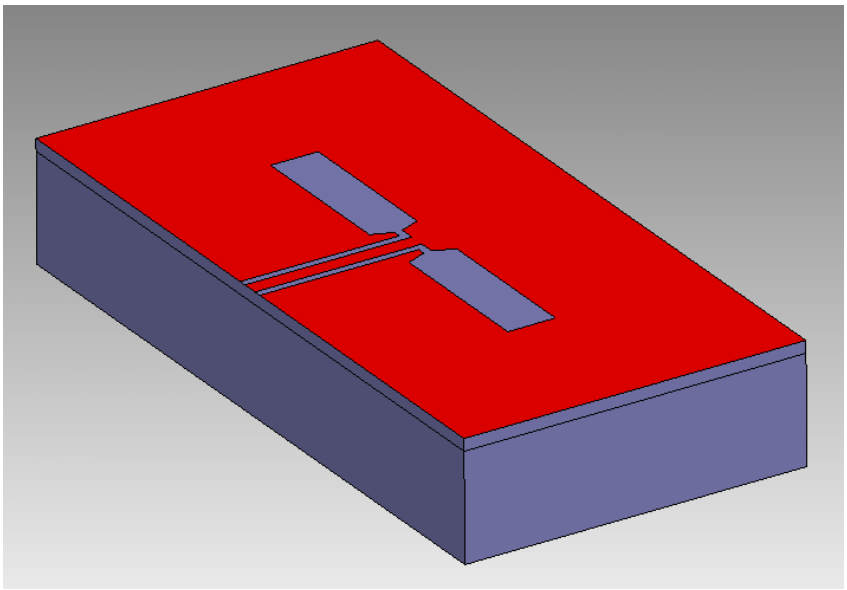

Figure 5.2 – Single Cavity-backed Slot

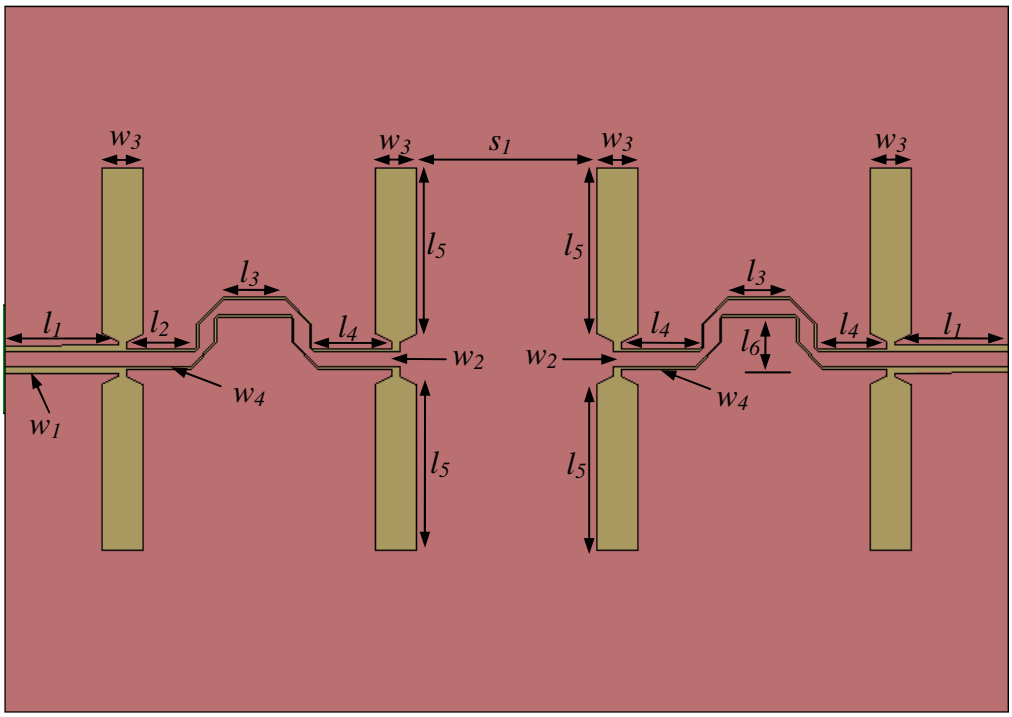

Figure 5.3 – Top View of Cavity-backed Array in HFSS.

Table 5.1 – Dimensions of Cavity-backed Array

Dimension	Length/width(mm)	Dimension	Length/width(mm)
l_1	14.5	s_1	23
l_2	8.75	w_1	0.75
l_3	7.93	w_2	2
l_4	10	w_3	5.2
l_5	21	w_4	0.26
l_6	6.12		

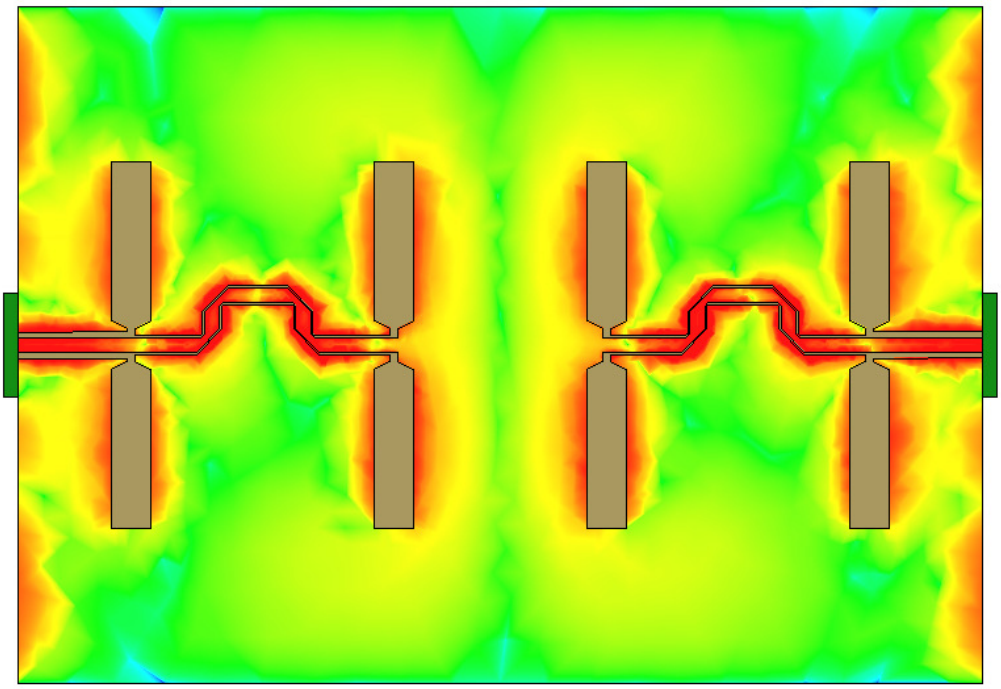

Figure 5.4 –Plot of Current Distribution for Final Cavity-backed Design.

Once more, the current plot in Figure 5.4 ensures that electrical length between the slots is one wavelength and the slots are excited in phase. The current distribution shown here indicates that the all four slots are radiating together and with nearly equal power.

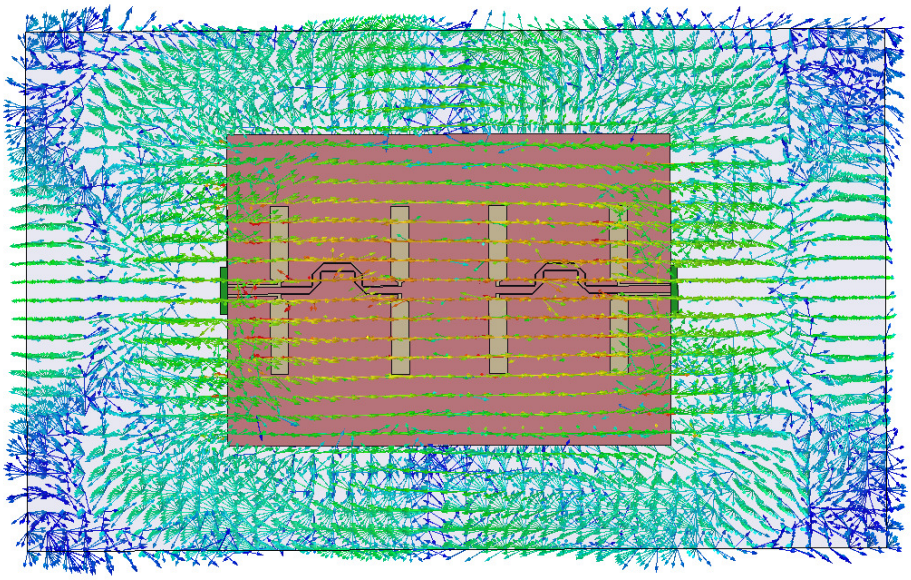

Figure 5.5 –Top View of E-field Vectors Surrounding the Cavity-backed Design.

Looking from above, the arrows of Figure 5.5 are representative of the E-field vectors surrounding the cavity-backed array. The fields above the array are linearly (horizontally) polarized along the direction of the slot's width and are strongest in the array's geometric center. The field vectors will always be horizontally polarized, but will flip directions (left-to-right or right-to-left) depending on the upward or downward cycle of the sinusoidal source. The field is also shown to exist far beyond the structure. Figure 5.6 shows that some fields also exist behind the cavity. The fields can be seen coupling from the front around to the back. The cavity appears to be effective in highly suppressing radiation in the backside.

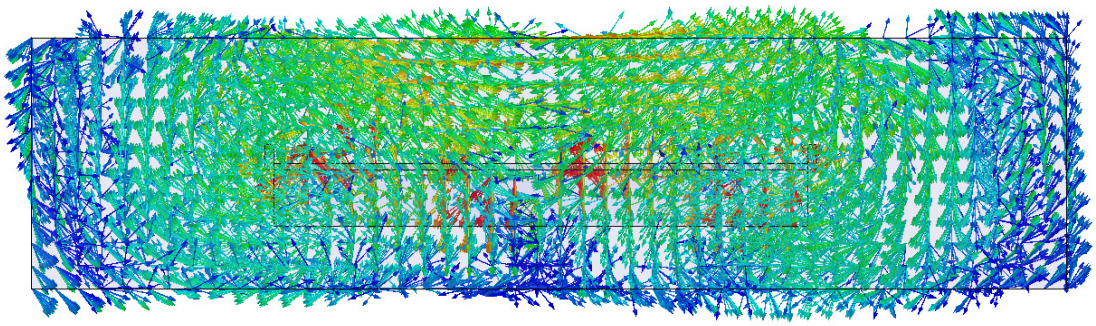

Figure 5.6 –Side View of E-field Vectors Surrounding the Cavity-backed Design.

To verify that the array symmetry and dual feeds will prevent beam-drift across frequencies, the gain of the array was plotted at center frequency and other, nearby frequencies.

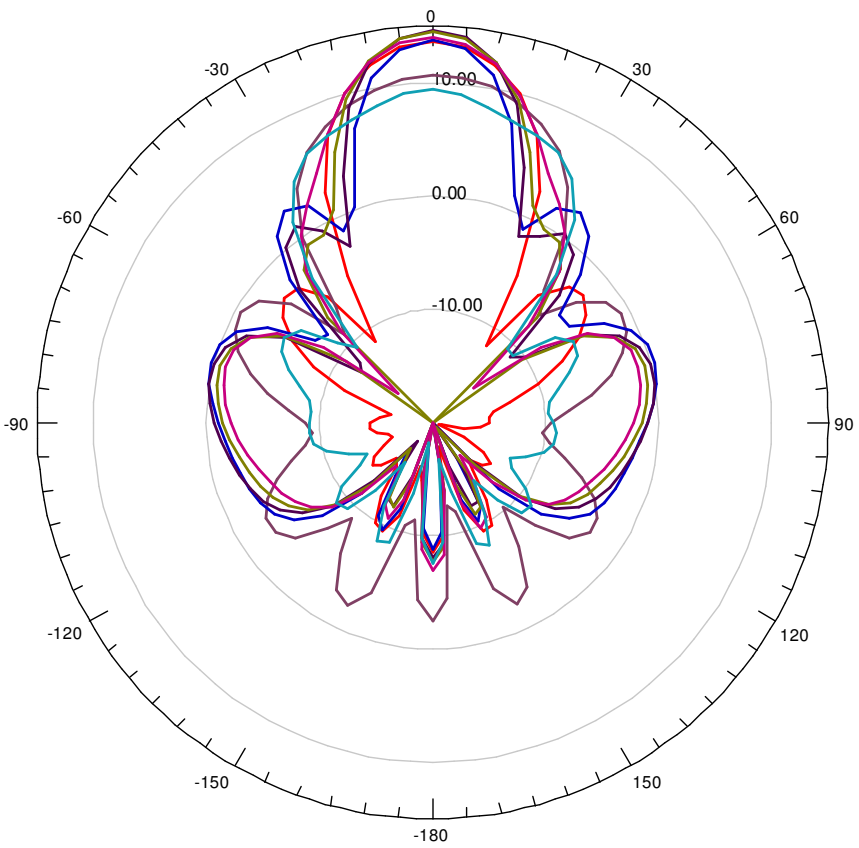

Figure 5.7 – E-Field Gain Over Multiple Frequencies.

The plots in Figure 5.7 corroborate this point. It should be noted that the major lobe of this array remains at broadside for all plotted frequencies (100MHz steps between 4.6-5.4GHz). The gain will degrade, though, in proportion to the departure in frequency away from f_c.

5.4 Results and Comparison

The design was again milled into a 60mil Rogers 4003C board (ε_r=3.55) and placed into an aluminum cavity. The cavity was designed such that the groundplane of the array was flush with the top of the cavity In Figure 5.8, the simulated RL bandwidth is ~360MHz BW (7.2%) and greater than 1.17GHz (23.4%) for the measured. In actuality, the RL for the measured design was > 10dB beyond 7GHz, but attention was kept at the established band of interest. The fabricated and simulated arrays both have deep resonances near 5GHz, but, otherwise, their RL features do not have much correspondence.

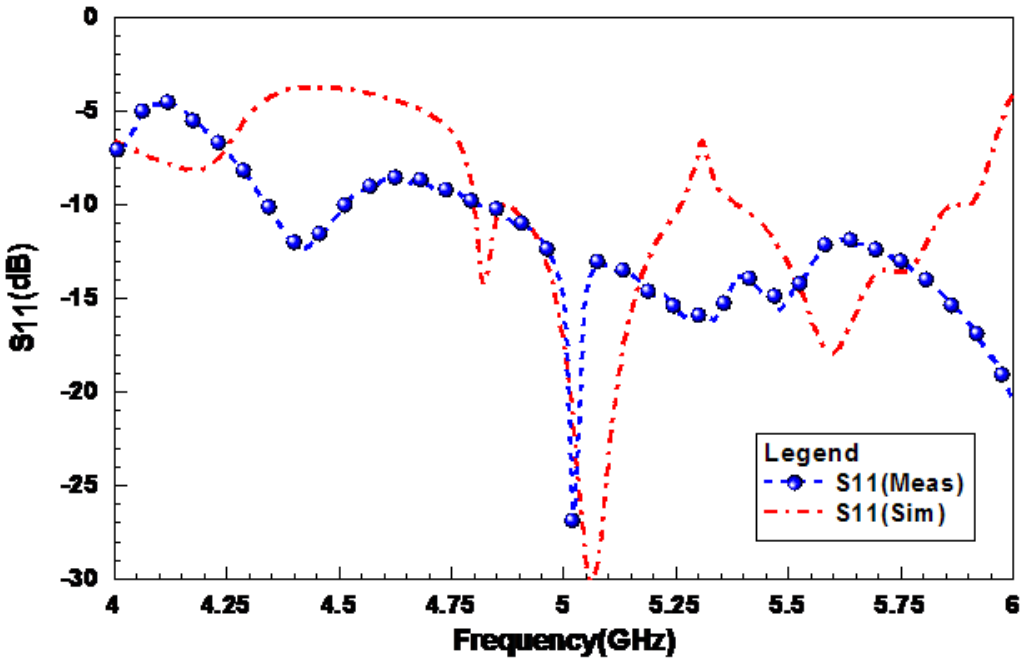

Figure 5.8 –Simulated vs. Measured Return Loss for Cavity-Backed Array

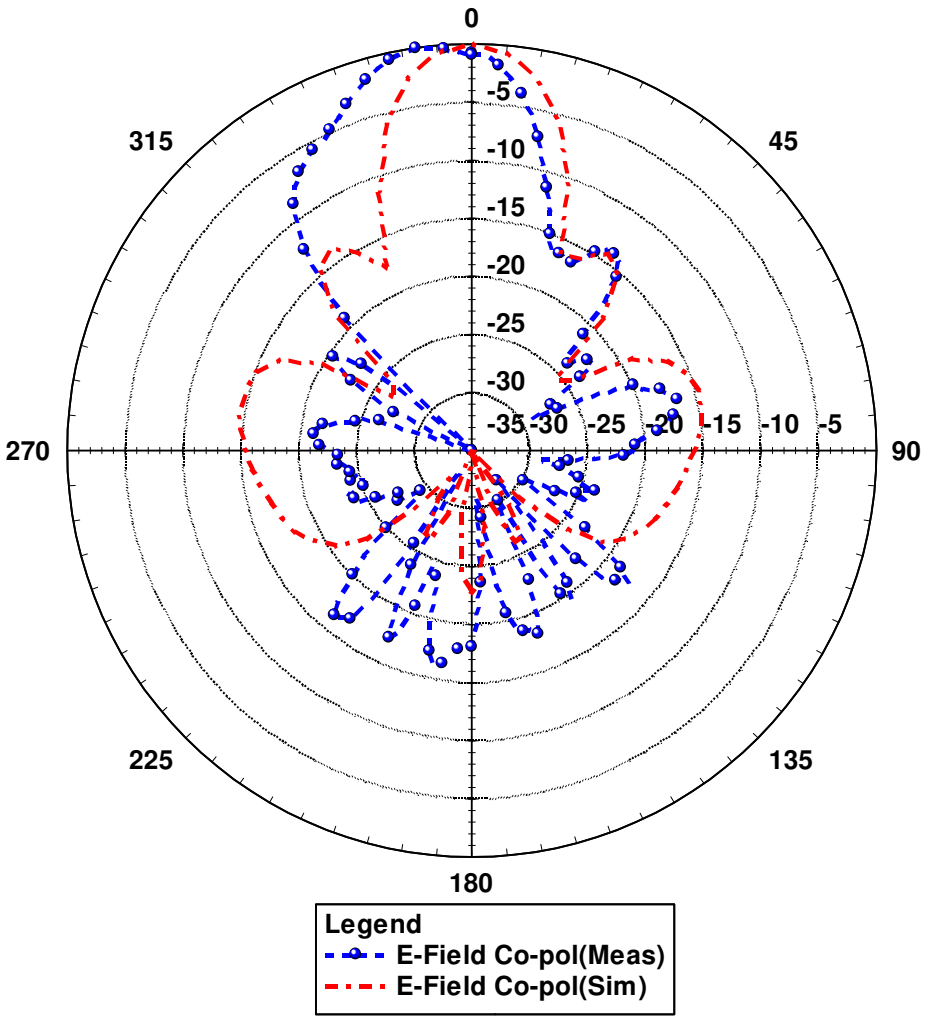

Figure 5.9 - Simulated E-Co. vs. Measured E-Co.

The gain of the simulated, cavity-backed antenna was 14.575dBi with sidelobes that were 14dB down. Measured gain was more than 3dB lower at 11dBi with sidelobes still about 14dB down. The E-field co-polarization plots in Figure 5.9 are largely in accordance, less the apparent anomaly in part of the major lobe. Rather than including the delay line in the design, one attached post-processing. The delay (including a 50Ω milled line and various coax connectors) was likely the cause of this discrepancy.

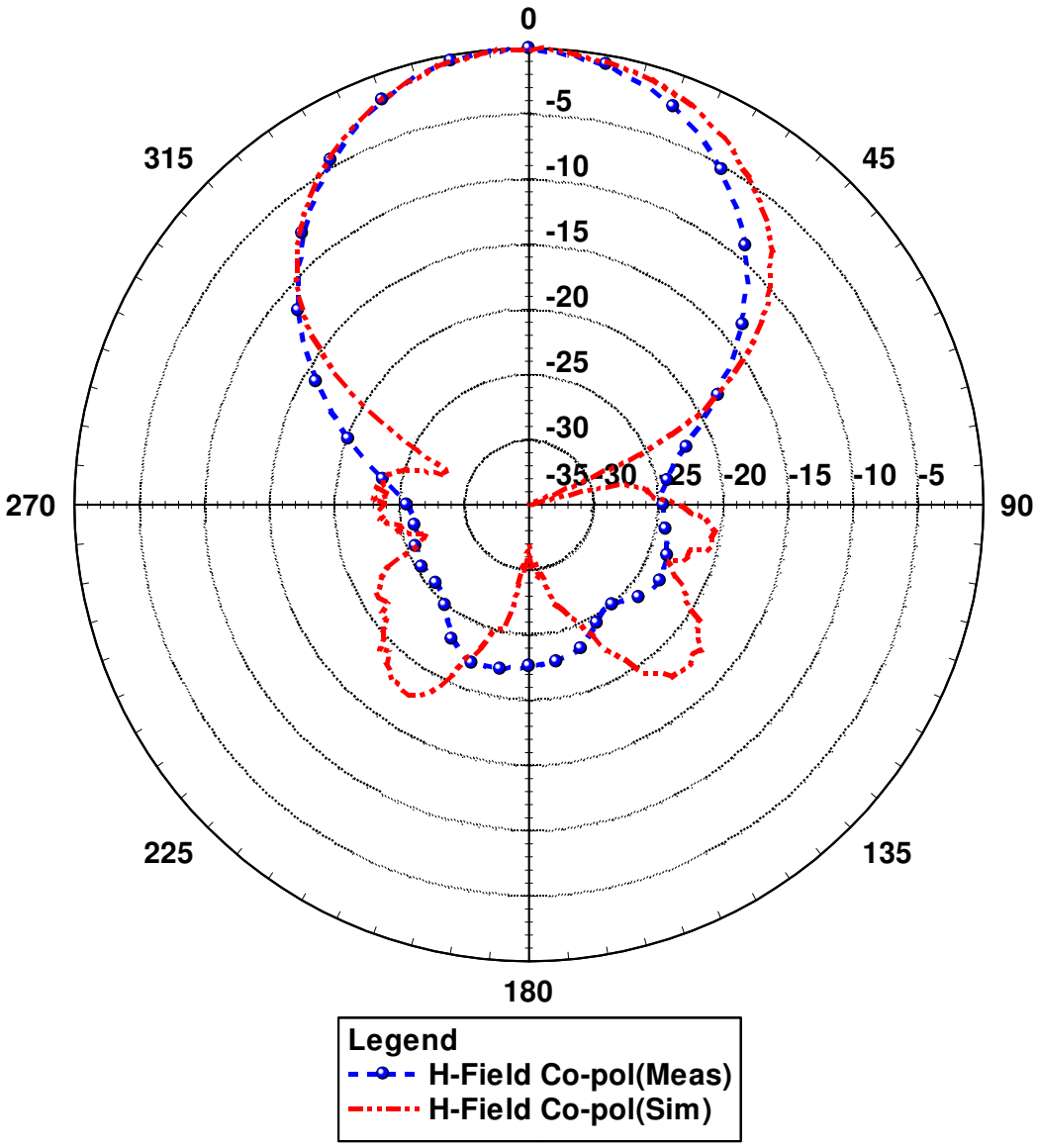

Figure 5.10 - Simulated H-Co. vs. Measured H-Co.

H-field co-polarization cuts demonstrate closer alignment and nearly identical beamwidths. Impedance or phase errors exposed in the E-plane (Figure 5.9) would be difficult to detect in the H-field. The array is only capable of beam-tilt in the E-plane, along the axis that the elements lay along. The width of the beam in the H-plane is set by the length of the slots and should never tilt.

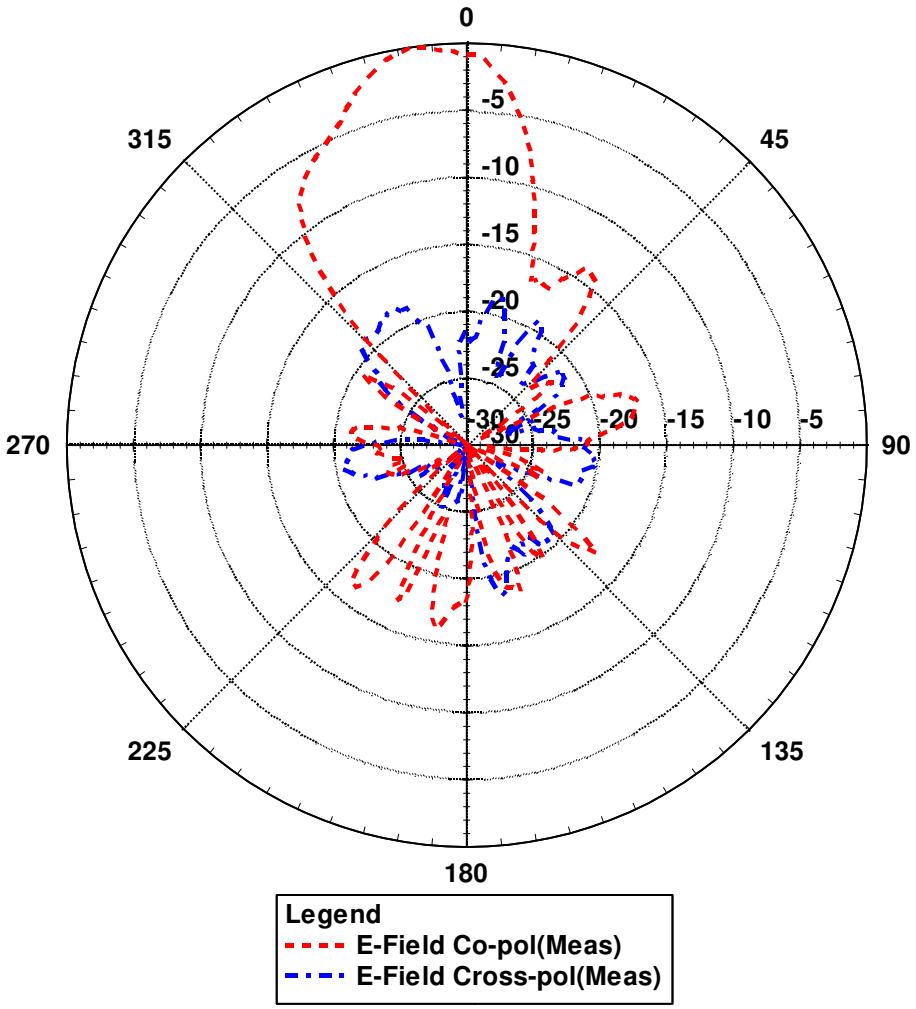

Figure 5.11 – Measured E-Co. vs. Measured E-Cross.

Both co-polarization plots show that backside radiation is ~18dB down from the major lobe. Figures 5.11 and 5.12 exhibit the array's extremely low cross-polarization levels for both E and H-planes.

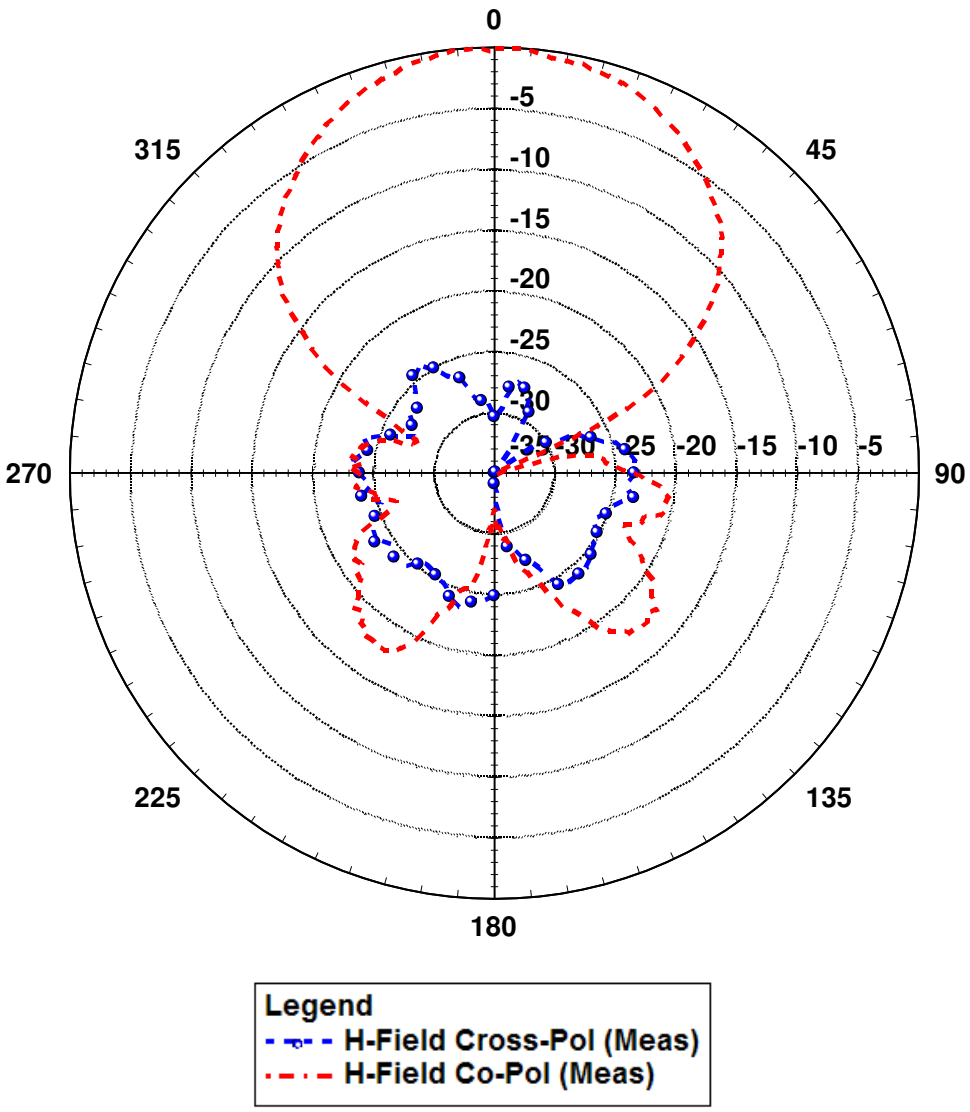

Figure 5.12 – Measured H-Co. vs. Measured H-Cross.

5.5 Chapter Summary and Conclusions

Through a straightforward design approach, a four-element slot array was tuned to function well within a metallic cavity. Some approximate assumptions could be made in the early design stages, but the complexity of the structure necessitates a 3-D solver like HFSS for reliable characterization. The array yielded a directive lobe at broadside, but

did suffer from some deformation; likely an incidental artifact of the phase-delay network on one of the ports. The broad lobe in the H-plane for measured and simulated arrays were in close agreement. Backside radiation levels were shown to be greatly suppressed, a direct benefactor to the frontside gain. And, the 8dBi of measured gain for the planar array (Chapter 4) was increased, as anticipated, by 3dB with the installation of the cavity.

CHAPTER 6

THESIS SUMMARY AND FUTURE WORK

6.1 Summary

This work demonstrated that a series-fed slot array with dual, anti-symmetric feeds can be designed to function within a metal cavity with improved gain. The four-element structure generates a single major lobe at broadside with 11 dB of gain and sidelobes which are14 dB down. Dual feeds, one at each end of the array, are pivotal in prohibiting beam-drift against frequency and were shown to function as expected. Each component of the antenna was considered theoretically as a starting point, then analyzed experimentally in software simulations. Finally, each step of the design was fabricated, measured and compared to its simulations.

The array was first constructed around a wavelength-long, rectangular slot. Each slot was designed to radiate with a center frequency of 5GHz and ~20% BW. To improve gain, a linear array of four such elements was capable of ~8dBi of gain and a bandwidth of +28%. That array was tuned to operate within a metallic cavity for an improved gain of ~11dBi.

Keeping with modern trends, the CPW-fed, slot array presents an efficient, low-profile and inexpensive approach for attaining bi-directional or uni-directional radiation, improved gain performance and radiation fixed at broadside over a range of frequencies.

This work seeks to make its small contribution to the bigger body of concurrent research. There is, no doubt, much room for improvement with this design. Suggestions are in 6.2.

6.2 Future Work and Recommendations

Throughout the process of developing this project, many questions arose. Entangled with these questions are many plausible solutions, only a few of which could be fully explored. The author could go on ad infitum in suggesting future work or citing useful enhancements for this project. A few of the more pertinent modifications will be named below.

The gain of the array could most readily be improved by expanding the array with additional elements. The series-fed structure is such that more elements could be simultaneously fed if the impedance of the lines was set to match their respective impedances. For increased the bandwidth, the bow-tie slot showed promising potential. It and other slot designs should be investigated further for bandwidth improvements.

To implement the scanning capabilities of this work, a phase shifter and/or power-splitting network is necessary. Phase shifters can be constructed in a number of ways but must address, in varying degrees, some issues like:

1.) Ability to change rapidly
2.) High peak and average power handling
3.) Low loss
4.) Insensitive to temperature changes
5.) Small in size and weight

Common to phased arrays for radar applications, diode phase shifters and ferrite phase shifters are potential candidates. The diode-flavored are digital devices which have discrete phase values while the ferrite shifters are analog and are driven by applying an external H-field.

Ultimately, the combination of many planar segments, like that designed here, could be arranged around a cylinder to form an omni-directional pattern (Figure 6.2).

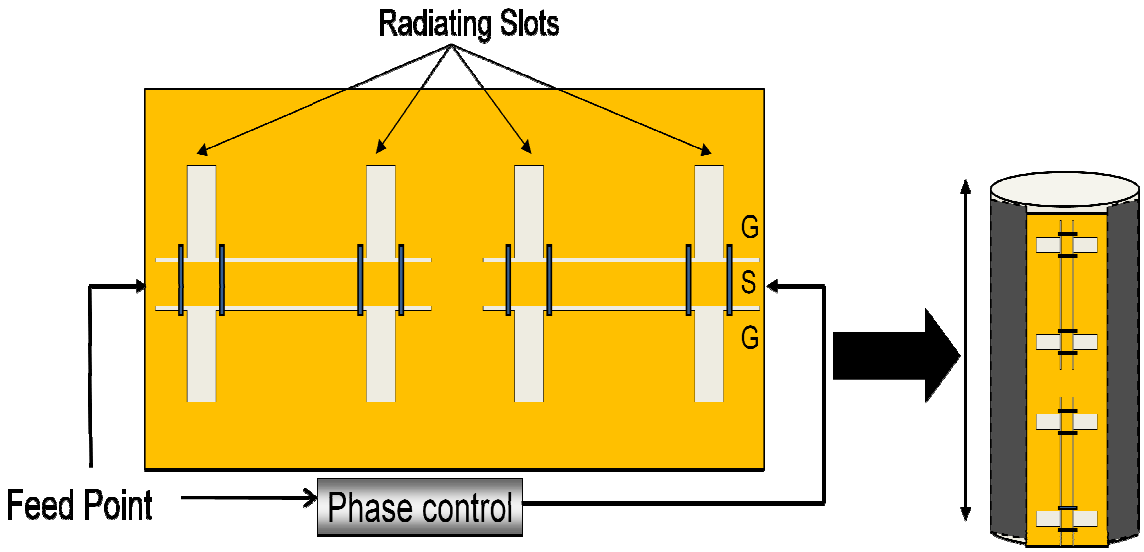

Figure 6.1 – Linear Array with phase shifter (a), Omni-directional Structure (b)

Each panel would make up a portion or slice of the total far field pattern. Coupled with a phase shifting network, each directive beam could scan vertically (as picture in Figure 6.1(b)). This concept is ideal for moving objects that are prone to tilt, lean, or pitch. The panels could be electronically steered to compensate for the movement of the vessel and keep radiation fixed in a particular direction. Additionally,

the design pattern allows each panel to be individually turned “on” or “off”, thus preventing any transmission or reception in a particular direction. This feature would be propitious in combating jamming attempts as the segment(s) undergoing jamming could be intentionally disabled.

REFERENCES

[1] Constantine A. Balanis, *Antenna Theory Analysis and Design,* 3rd ed., John Wiley& Sons, Inc., Hoboken, New Jersey, 2005.

[2] W.L. Stutzman, G.A. Thiele, *Antenna Theory and Design,* John Wiley and Sons, New York City, New York, 1981.

[3] W.H. Watson, *The Physical Principles of Waveguide Transmission and Antenna* Systems, Clarendon Press, Oxford, 1947.

[4] A.F. Stevenson, "Theory of Slots in Rectangular Waveguides," J. Appl. Phys., Jan. 1948, pp: 24-38.

[5] M. Orefice, **"**Design of waveguide-fed series slot arrays," IEEE Proceedings, Vol.129, Pt. H, No. 4, Aug. 1982, pp: 165-169.

[6] L. Goldstone, A. Oliner, "Leaky-Wave Antennas I: Rectangular Waveguides," Antennas and Propagation, IRE Transactions on**,** Vol. 7, Iss. 4, Oct. 1959, pp: 307-319.

[7] F. J. Paoloni, "A Cavity-Backed Resonant Slot Array-Theory and Measurement," Antennas and Propagation, IEEE Transactions on, Vol. AP-28, No. 2, March 1980, pp 259-263

[8] Increased-bandwidth Resonant Slot Aarray with Bidirectional Radiation Pattern, Electronics Letters Sept. 1974, Vol. 10 No. 19, pp:396-397.

[9] Y. Yoshimura, **"**A Microstripline Slot Antenna," Microwave Theory and Techniques, IEEE Transactions on, Vol. 20, Iss. 11, Nov. 1972, pp:760-762.

[10] A. Nesic , "Slotted Antenna Array Excited by a Coplanar Waveguide," Electronics Letters, Vol. 18, No. 6, March 1982, pp: 275-276.

[11] E.A. Soliman,et al., **"**Bow-tie Slot Antenna Fed by CPW," Electron. Lett., Vol 35, 1999, pp: 514-515.

[12] Y.D Lin, S.N. Tsai, "Coplanar Waveguide-Fed Uniplanar Bow-Tie Antenna," Antennas and Propagation, IEEE Transactions on, Vol. 45, No. 2, Feb 1997, pp:305-306.

[13] M. Nedil, T.A. Denidni, L. Talbi, "A New Back-to-Back Slot Bow-Tie Antenna for Millimeter-Wave Applications," IEEE CCECE Canadian Conference, Vol. 3, May 2003, pp: 1433-1436.

[14] C.H.Lee, S.-Y. Chen, P. Hsu, "Compact Modified Bow-tie Slot Antenna Fed by CPW for Ultra-wideband Applications," IEEE AP-S International Symposium and URSI Radio Science Meeting, Jun. 2009.

[15] L. Marantis, P. Brennan,"A CPW-Fed Bow-tie Slot Antenna with Tuning Stub," Antennas & Propagation Conference, March 2008, pp:389-392.

[16] S.-Y Chen, P. Hsu, "A Modified Bow-tie Slot Antenna Fed by a Coplanar Waveguide," Antennas and Propagation, IEEE Transactions on, Vol. 1, June 2004, pp:799-802.

[17] S.-H. Wi, J.-M. Kim, et al., "Bow-tie-shaped Meander Slot Antenna for *5* GHz Application," Antennas and Propagation, IEEE Transactions on, Vol. 2, 2002, pp:456-459.

[18] Y.-L. Chen, C.-L. Ruan, L.Peng, "A Novel Ultra-wideband Bow-tie Slot Antenna in Wireless Communication," Progress In Electromagnetics Research Letters, Vol. 1, 2008, pp:101–108.

[19] A. Bhobe, **"**Wide-Band Slot Antennas with CPW Feed Lines: Hybrid and Log-Periodic Designs," Antennas and Propagation, IEEE Transactions on, Vol.52, No.10, Oct. 2004, pp: 2545-2554.

[20] H. Kobayashi, **"**Slot Array Antennas Fed by Coplanar Waveguide for Millimeter Wave Radiation," Microwave Theory and Techniques, IEEE Transactions on, Vol.46, No. 6, 1998, pp: 800-805.

[21] T.F. Huang, S.W. Lu, P. Hsu,"Analysis and Design of Coplanar Waveguide-Fed Slot Antenna Array," Antennas and Propagation, IEEE Transactions on, Vol. 47, No. 10, Oct. 1999, pp:1560-1565.

[22] S.Y. Chen, I.C. Lan, P. Hsu, "In-Line Series-Feed Collinear Slot Array Fed by a Coplanar Waveguide," Antennas and Propagation, ," IEEE Transactions on,Vol. 55, No. 6, June 2007, pp:1739-1744.

[23] R.E. Collin, *Antenna Theory Part 1,* 3rd ed., McGraw-Hill, Inc., Hoboken, New York, 1969

[24] C. Huygens, "Traite de la Lumiere, Leyde," 1690. Translated into English by S.P. Thompson, London, 1912, reprinted by The University of Chicago Press.

[25] R. Garg, P. Bhartia, I. Bahl, A. Ittipiboon, *Microstrip Antenna Design Handbook*, Artech House, Norwood, MA, 2001, Ch 7.

[26] Robert E. Collin, *Antenna Theory Vol. 7*, McGraw-Hill Book Company, Hoboken, New York, 2005.

[27] L.V. Blake, *Antennas* Norwood, Artech House, MA 1984.